Walker: A Simple Millipede Bot

Thesis submitted in partial fulfillment of the requirements for the degree

of

Bachelor of Science in Robotics Engineering

by

Kyle Jeffrey
1675663

Under the supervision of

Prof. Steve McGuire

DEPARTMENT OF ELECTRICAL AND COMPUTER ENGINEERING

UNIVERSITY OF CALIFORNIA SANTA CRUZ

SPRING 2021

DECLARATION

Project Title	Walker: A Simple Millipede Bot
Author	*Kyle Jeffrey*
Student ID	1675663
Supervisor	Prof. Steve McGuire

I declare that this thesis entitled *Walker: A Simple Millipede Bot* is the result of my own work except as cited in the references. The thesis has not been accepted for any degree and is not concurrently submitted in candidature of any other degree.

Kyle Jeffrey
1675663

Department of Electrical and Computer Engineering
University of California Santa Cruz

Date: June 6, 2021

Department of Electrical and Computer Engineering
University of California Santa Cruz
Santa Cruz, California

CERTIFICATE

This is to certify that the thesis entitled **Walker: A Simple Millipede Bot**, submitted by **Kyle Jeffrey** (Student ID: 1675663) an undergraduate student of the **Department of Electrical and Computer Engineering** has been examined. Upon recommendation by the examination committee, we hereby accord our approval of it as the presented work and submitted report fulfill the requirements for its acceptance in partial fulfillment for the degree of *Bachelor of Science in Robotics Engineering*.

Prof. Steve McGuire
Assistant Professor

Department of Electrical and Computer Engineering
University of California Santa Cruz

Prof. Gabriel Elkaim

Department of Electrical and Computer Engineering
University of California Santa Cruz

Place: Santa Cruz
Date: June 6, 2021

ACKNOWLEDGEMENTS

I feel deep gratitude for those that carried me throughout this process. They were the many legs that carried my research. My research supervisor, *Prof. Steve McGuire*, was an invaluable guide, and I would not have finished this paper without him. Without attending *Prof. Mircea Teodorescu's* Bio-locomotive Inspired Design course I never would've pursued this study.

I'd to like to thank *Dr. Anthony Garcia* for being my north star, and introducing me to the vast, complex study of millipede locomotion. His many publications on the matter were a primary source for this paper.

Lastly I'd like to thank my parents for lending an ear to my technical strife throughout this research. Without them I surely would've fallen short of the finish line.

Kyle Jeffrey
University of California Santa Cruz
Date: June 6, 2021

Dedicated to
Sidnie Manton's outstanding contribution to Zoology

– Kyle Jeffrey

ABSTRACT

Within the field of robotics, there is a demand for robots capable of atypical terrain traversal. Atypical environments like stairs, rocky trails, and off-road locations consist of chaotic, non-flat terrain that ordinary wheeled robots struggle to cross. Companies like Boston Dynamics have developed humanoid and animal-like robots capable of traversing such terrain; however, these robot designs are expensive and complicated. Using biological inspiration from millipedes and centipedes, this paper aims to develop a cost-effective and easily reproducible design to solve the problem of traversal through diverse terrain.

The development of the design, titled Walker, included research into the biology of millipedes and centipedes, a review of existing literature on insect-inspired leg actuators, implementation of an existing cam actuator by Wan and Song [19], and development of a simulation environment tested by hardware implementation. The outlined procedures were completed at home in novel, affordable ways due to the COVID-19 Pandemic.

Keywords: Millipede, Centipede, leg actuators, Robotics

Contents

List of Figures

List of Tables

Chapter 1

Introduction

1.1 Problem Statement

The need for robots capable of maneuvering uneven terrain grows yearly as simple wheel design robots are often limited in their capability to do so. In response, the field of bio-locomotive design looks to nature for inspiration. The field considers animals as robust, dynamic movement systems evolved precisely for their habitat. Existing studies have investigated the particular robust locomotive characteristics of millipedes and centipedes as motivation for solving chaotic terrain traversal. These many-legged insects cross diverse habitats and present a simple, easy to emulate, and highly modular body structure. My research expands upon present analytical literature on the locomotive mechanisms of millipedes and centipedes as robotic inspiration. Though previous papers have attempted to recreate the omnipede platform by emulating their characteristic behavior, the resulting robot designs often use numerous motors for each body segment and complicated control schemes, decreasing the ease of reproduction. The Walker robot this paper designs builds a simplified omnipede robot inspired by existing studies and utilizes the advantageous characteristics of the Myriapoda.

1.2 Existing Millipede Mimetic Robot Investigations

There are numerous studies and implementations of omnipede robots. Literature review of these studies primarily focused on millipede-type mimicry for design inspiration. Below is a list of the most cited sources in the development of Walker.

1. ”Millipede-Inspired Locomotion for Rumen Monitoring through Remotely Operated Vehicle” By Garcia [7]

2. ”Centipede Robot for Uneven Terrain Exploration: Design and Experiment of the Flexible Biomimetic Robot Mechanism” by Koh et al. [10]

3. ”Decentralized control mechanism underlying interlimb coordination of millipedes” by Kano et al. [9]

4. ”The Kinematic Design of the OmniPede: A New Approach to Obstacle Traversion” Long et al. [11]

Special attention was given to the many works by Garcia et al. [5][7][6]. His publication extensively covered millipede gait kinematics as well as the production of millipede-like robots. His correspondence with me was an excellent source of guidance, as was his 2015 dissertation[5], the primary source of my investigation of millipede locomotion and robot development.

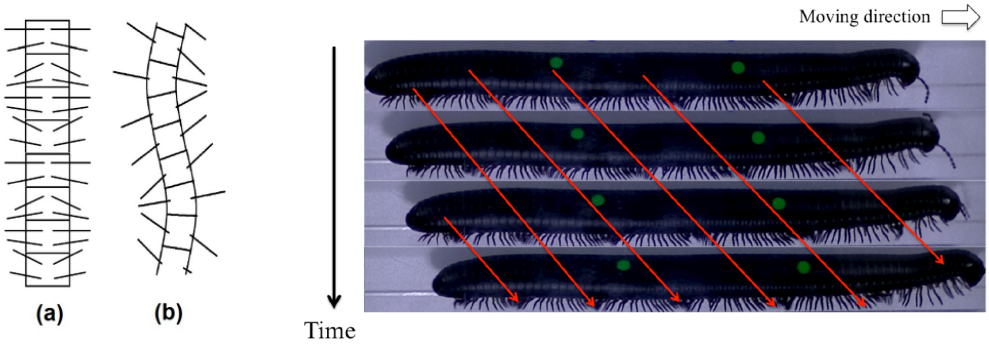

Figure 1.1: From [5] and [9]. (Left) Difference in gait - a) millipede b) centipede, (Right) Metachronal wave propagating through legs. Lines track points of travelling wave. Millipedes lack lateral undulation across their bodies, that centipedes implement for greater speed

1.3 Characteristics of a Millipede

Throughout the paper, the Myriapoda is referred to when referencing the insect species. The term omnipede is a placeholder for all abstracted robots that imitate the Myriapoda.

Millipedes and centipedes are well-documented insects. The zoological studies surveyed in this paper included Manton [12][13], Hopkin et al. [8], Wilson [20], and Minelli [14][15]. In zoological taxonomy, these insects fall into the Myriapoda classification meaning "many-legged ones". Millipedes, classified as Diplopoda, and centipedes, Chilopoda[14], are primarily distinguished by key locomotive and anatomical differences.

Regarding the research goal of developing a simple robot platform, the critical difference between these subgenus' is leg motion. Millipede leg trajectory has been modeled along a geometrically simple, 2-axis trajectory with relative accuracy (see Section 2.1.1). The millipede's body suspends statically in the air as it moves forward. In contrast, the centipede's gait involves complexity in leg movement and lateral oscillatory body movement. The static body and leg movement of the millipede make it the primary inspiration for research.

The Myriapoda maintains consistent stability traversing uneven terrain primarily because of the many legs. Both insects incorporate a wave-like motion that propagates through the legs when traversing(see Fig. 1.1). This wave-like phenomenon in the legs is an effect of metachronal gait(see Parker and Mills [16]). A metachronal rhythm is not a Myriapoda-specific gait pattern, but in the Myriapoda, it manifests through a sequential movement of legs. This locomotive pattern means that legs lift only when neighboring legs contact the ground to provide support. Kano et al. [9] reviewed metachronal gait vis-a-vis the millipede system through study and production of a closed feedback millipede robot. Both the millipede and centipede share this wave-like undulation across their legs. However, the metachronal wave propagating through the right and left side of the millipede legs are in phase with each other, while the centipede's traveling waves are 180° out of phase as displayed in Fig. 1.1. This difference in phase and lateral undulating locomotion[1] cause most centipedes to move faster than millipedes. However, what the millipede lacks in speed, it compensates in thrust capabilities for burrowing as explored by Garcia [7], Manton [12]. The subsequent sections overview the leg anatomy and gait of the millipede.

1.3.1 Millipede Leg Anatomy

There is a difference in the leg structures among the many subspecies of the Myriapoda, but broadly speaking, they tend to have more than a few leg segments[15].

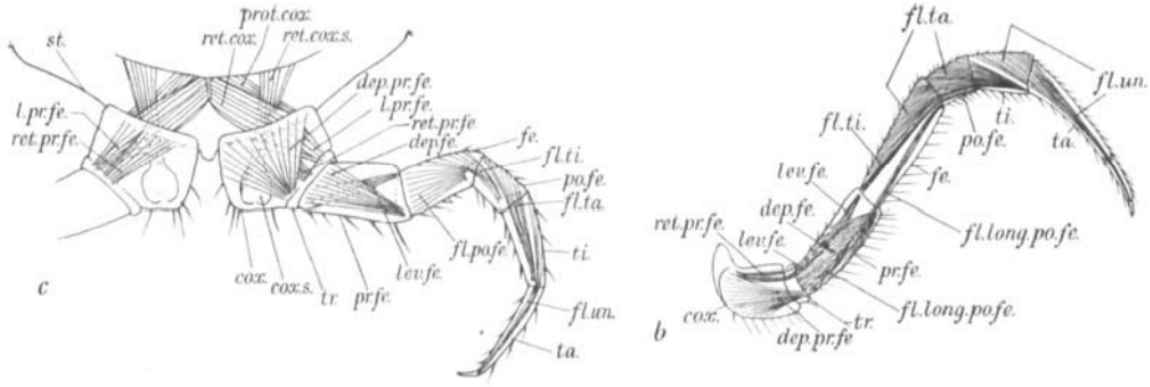

Figure 1.2: From Manton [12], Polyzonium Germanicum (common name Kentish Pin-head) leg structure. Millipede leg has many muscles for controlling movement but its motion is relatively simple.

Fig. 1.2 shows the many leg structures that the Kentish Pin-head Millipede has, but Manton [12] notes that most add no further motion and are almost entirely rigid. With many segments across a single leg, the trajectory of each leg occurs across all three positional axes. In other words, a single motor-controlled actuator cannot precisely emulate the trajectory. Notwithstanding, the trajectory can be mostly represented with simple kinematic equations, discussed further in Section 2.1.1.

1.3.2 Gait Analysis

The millipede is unique in its ability to manipulate gait to modulate thrust and speed. Manton [12] recognized this in her analysis on the shift of legs in backstroke to forward-stroke (see Fig. 1.4). The wavelength of the metachronal wave that propagates through the millipede's legs is a more apt description of the changing dynamics of millipede gait. The comparison between the number of legs in back-stroke to forward stroke also referred to as the ratio of legs in the propulsive state to legs in transfer state(see Fig. 1.3), is an effect of the changing metachronal wave.

This shift in the wave characteristics can be described even more simply by the change in the legs' 'duty cycle,' i.e., the time a leg spends in the air divided by the time a leg spends on the ground. In Garcia et al. [5]'s dissertation, he finds that the duty cycle is the same across all legs, and the millipede does little to change the angular velocity of its moving legs. Garcia finds that changing the duty cycle

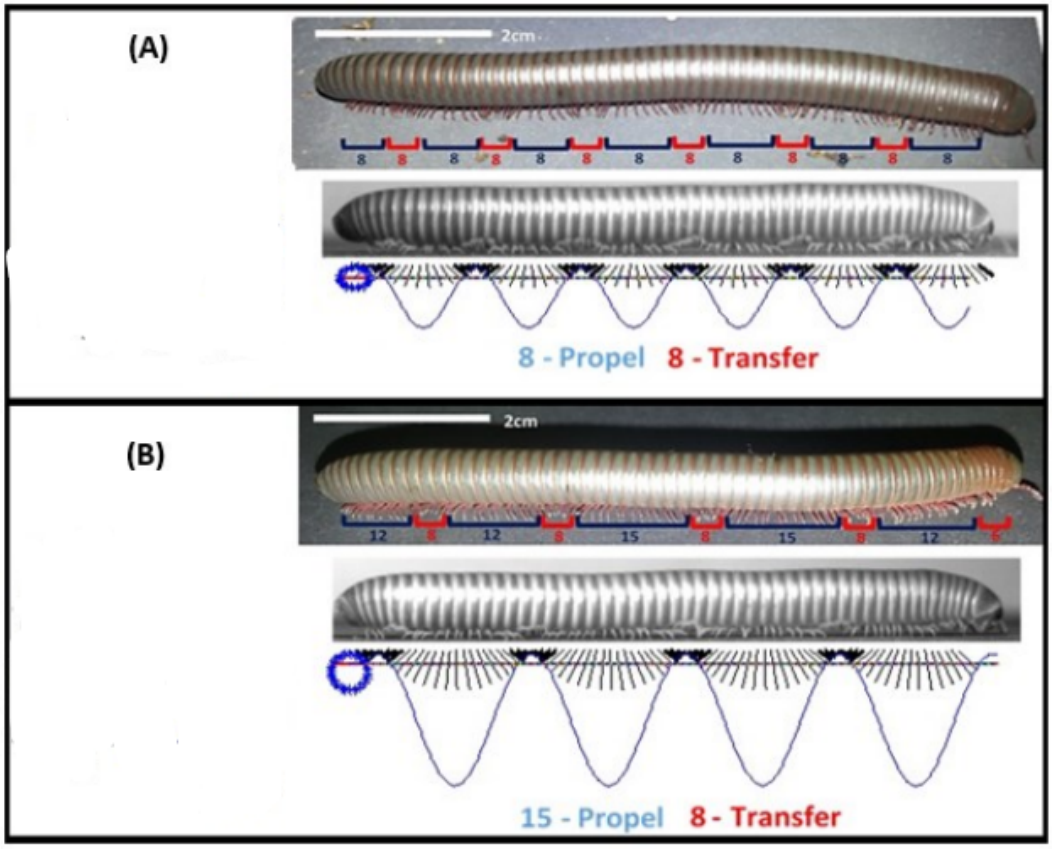

Figure 1.3: From Garcia [7], (A) 'high gear' gait, (B) 'low gear' gait, the more feet in propel, the greater the thrust but lower speed. The greater number of legs in propulsive is an effect of a higher duty cycle which generates greater thrust.

of legs determines the wave characteristics and thrust behavior. Modulating the duty cycle changes the millipede's 'gears,' much like a gearbox does. The millipede shifts between a 'low gear' mode with high thrust ability (duty cycle ≈ 0.7) and a 'high gear' mode with high speed (duty cycle ≈ 0.3). These 'gear modes' were also acknowledged by Manton [12] (see Fig. 1.4).

1.3.3 Why Millipedes?

The millipede maintains a constant body length throughout its gait, making it a relatively easy system to mimic with hard body materials. The entirety of its gait modulation is due to the characteristics of the metachronal wave propagating through its legs. Considering that the millipede maintains a rigid body structure throughout its gait and can maneuver across varied environments, it presents a

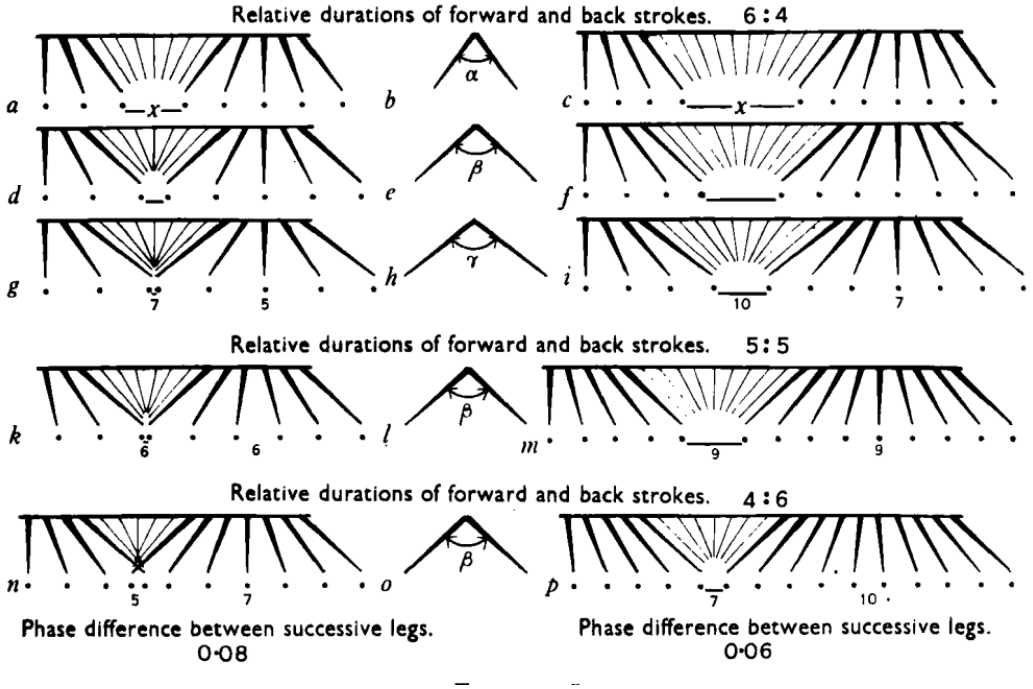

Figure 1.4: From Manton [12], duration of forward to back stroke characteristically changes metachronal wave. Millipedes shift their gait to create thrust or speed. 6:4 ratio represents time legs spend in forward stroke to backstroke. Phase difference between neighboring legs is also affected by this shift in duty cycle.

system with great potential for robotic emulation. Developing Walker to mimic the locomotive mechanics of millipedes should then beget the benefits of chaotic terrain traversal that millipedes possess.

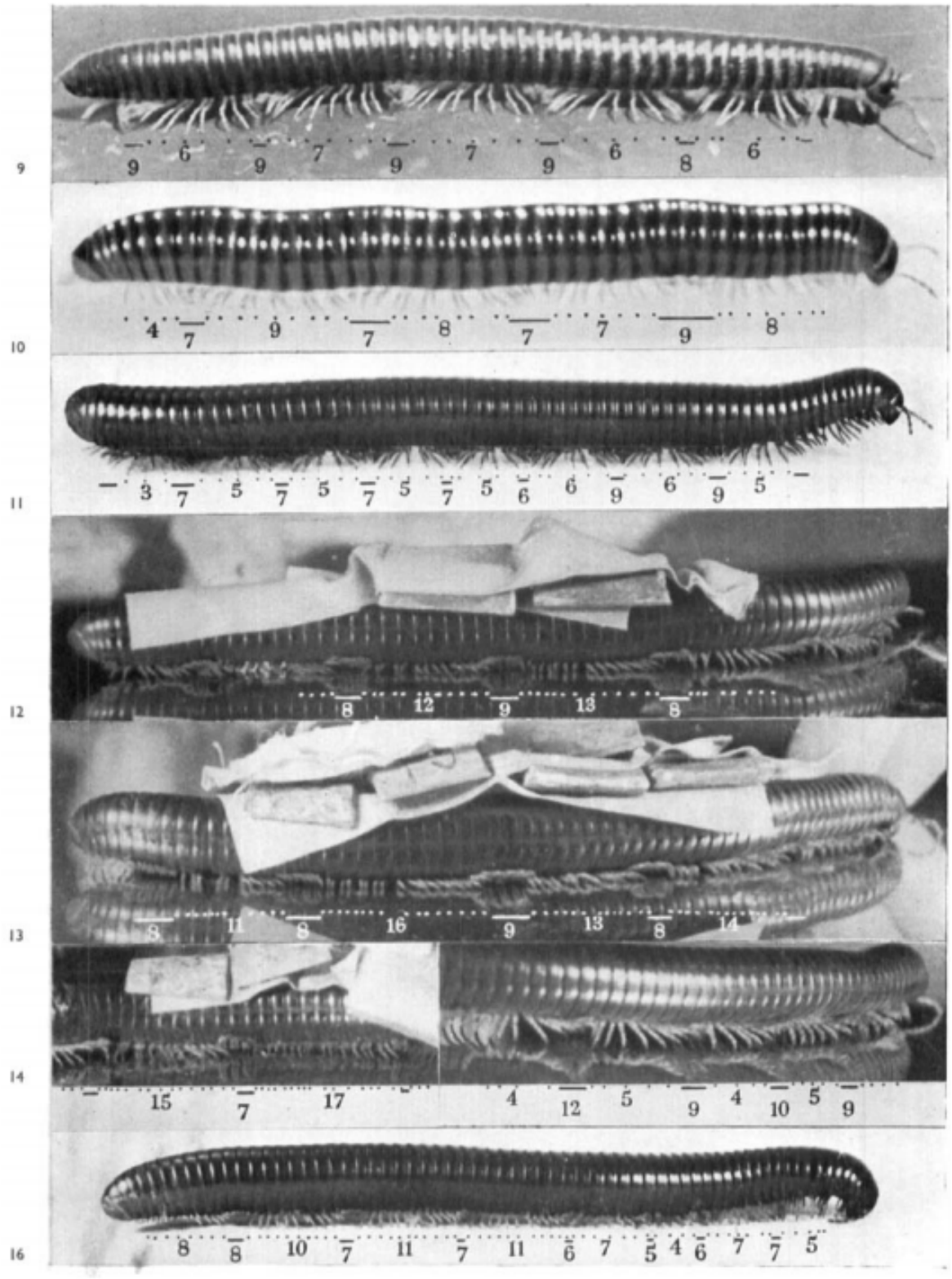

Figure 1.5: From Manton [12], duty cycle difference invoking different gaits of millipedes

Chapter 2

Kinematic Model

Before producing an omnipede robot, this chapter surveys the existing literature on millipede motion and derives a system of kinematic equations for modeling the movement of the Walker robot. The kinematic model describes the motion of omnipedes to be mimicked by Walker, independent of inertial considerations. Reviewing the academic literature did not reveal any system of dynamics equations for modeling these metachronal wave-based insects, so Chapter 4 considers the dynamics of motion using a 3D simulation developed in Matlab.

2.1 Literature Review

As described in Section 1.3.1, the legs of a millipede can be modeled on a two-dimensional plane and assumed to maintain the same trajectory. Other studies explored this reductive model of the real locomotive pattern and garnered working locomotive robotic systems. This simplified kinematic system is shown to be effective by Koh et al. [10], Garcia [7], and Long et al. [11].

Despite the simplicity of leg motion, the kinematics of the metachronal wave persisting through the legs of Myriapoda proves to be rather complex. The Myriapoda constantly shifts its metachronal gait to traverse the diverse geography of the landscape it crosses. Kano et al. [9] did develop a complicated multi-motor, multi-sensor robot to emulate the actuation of the millipede's metachronal wave through sensory feedback systems. However, his robot is not based on any kinematic description of the millipede's gait and rather focused on actuation through feedback. Creating a complex robot is beyond the scope of the Walker robot. Since there

exists no uncomplicated kinematic model for metachronal rhythm, the analysis of metachronal kinematics is reduced to a primarily qualitative description.

The following survey of kinematic models divides the kinematic analysis of millipede locomotion into a mathematical description of individual leg kinematics and a qualitative understanding of a millipede's metachronal gait.

2.1.1 Kinematics of the Millipede Leg Motion

The first consideration of the millipede's gait involves individual leg kinematics. A mathematical model is described by Sathirapongsasuti et al. [18] and explored further by Garcia et al. [5]. The system by Sathirapongsasuti et al. [18] defines a kinematic model of millipede leg motion based on three simplifying assumptions:

1. The number of millipede leg segments is one, though actual millipede legs have several segments
2. Every leg shares a common motion pattern
3. The tip of millipede legs traces out a circle; When it walks on the floor, the circle traces (called the circle of reference) is trimmed to a segment of the circle. See Fig. 2.1

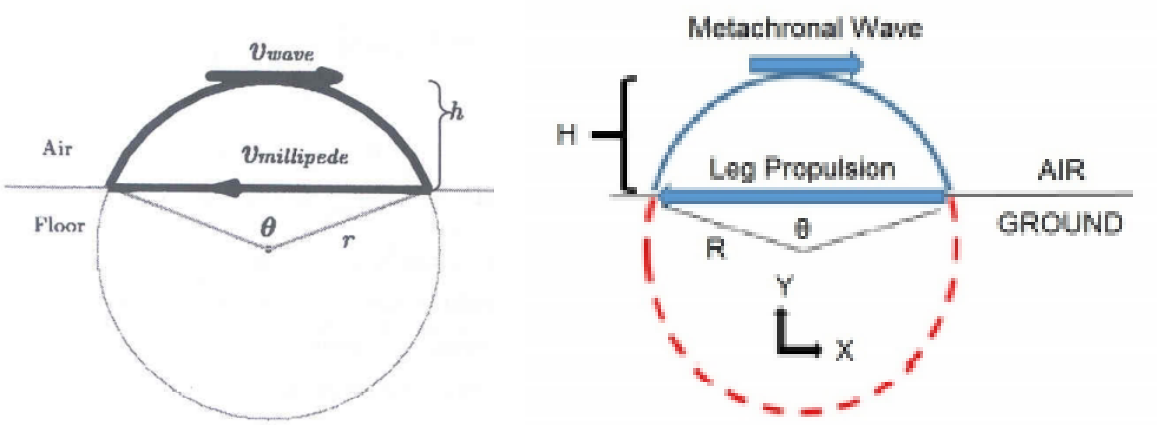

Figure 2.1: From [18](left) and [5](right), The circle of reference. The black path shows the path along which the tip of the leg traces. The red path shows the cut out segment which is skipped as the leg moves into the propulsive state.

With these three assumptions, the theoretical math is greatly simplified and provides a representative model of the millipede movement. Garcia [7] proves the

model is representative of millipede motion with After Effects analysis (see Fig. 2.2). The half-circle trajectory of the foot traces out a cycloid when moving forward, shown in Fig.2.2(c).

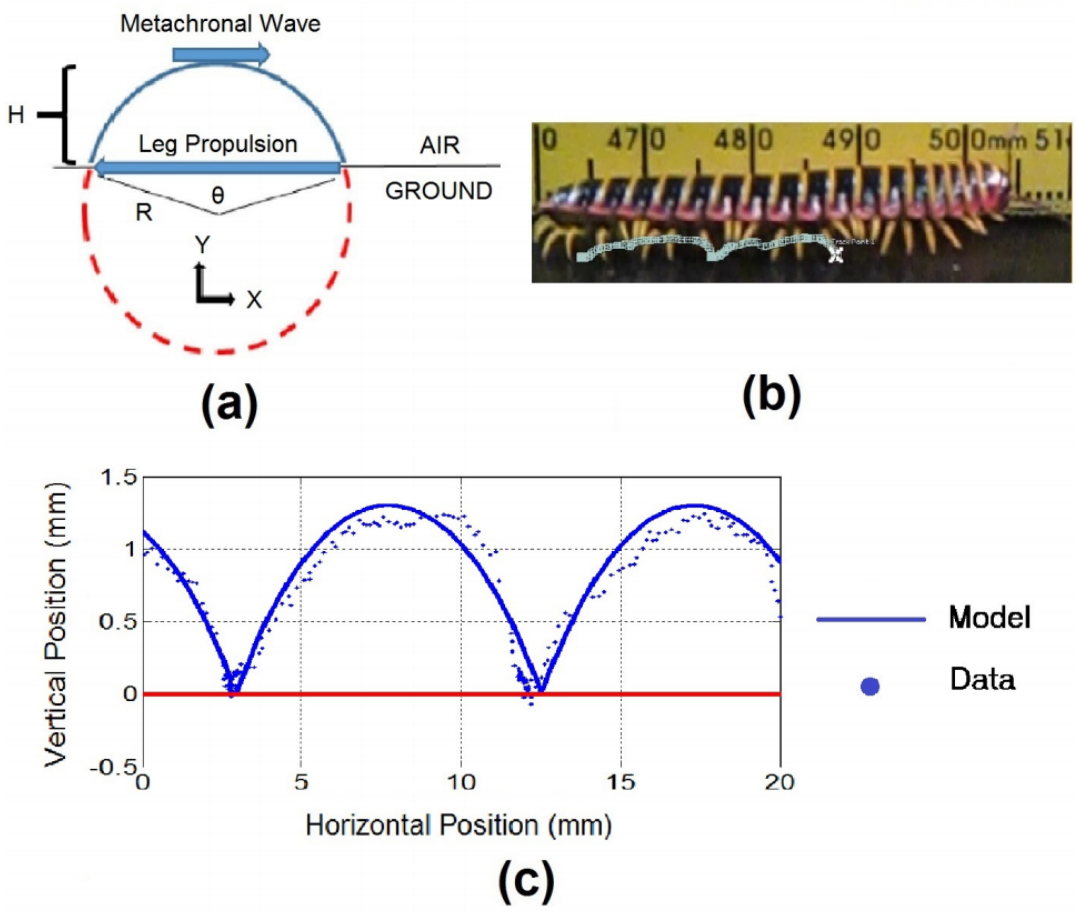

Figure 2.2: From [7] Video analysis shows the Sathirapongsasuti et al. [18] model of leg motion is representative of millipede leg motion. (a) Shows the circle of reference the individual feet follow along, (b) shows a snapshot of After Effects visually tracking a single leg motion, (c) compares the After Effects tracking data to the idealized cycloid path the legs follow

This model for the leg trajectory is standard in bio-inspired robot design and is often used in robotics to describe any poly-pedal system (see Raibert [17]). The trajectory of the leg as it moves along the circle of reference (see Fig. 2.1) divides into two phases: transfer and propulsive. In the transfer phase, the leg is lifted and moves forward along the arc of a circle, and in the propulsive phase, the leg is in

contact with the ground pushing the body forward by moving backward on the straight line.

Equations of motion are proposed by Sathirapongsasuti et al. [18] that describe the position of each leg based upon the duty cycle (the transfer time divided by propulsive time) and the radius of the circle of reference. Variables T_t for transfer time, T_p for propulsive time and R for radius of the circle of reference.

$$V_{wave} = \frac{\theta R}{t_T} \tag{2.1}$$

$$V_{millipede} = \frac{2Rsin(\theta/2)}{t_p} \tag{2.2}$$

$$T = t_T + t_p \tag{2.3}$$

$$H = R - Rcos(\theta/2) \tag{2.4}$$

$$\omega = \frac{\theta}{T - \frac{2Rsin(\theta/2)}{V_{millipede}}} \tag{2.5}$$

Where V_{wave} represents the velocity of the traveling metachronal wave, $V_{millipede}$ is the velocity of the millipede, and H is the clearance height of the leg, in addition to the aforementioned variables. Solving these equations for position:

$$x(t) = \begin{cases} V_{millipede}(t - \phi_t) - R\sin(\omega(t - \phi_t)) & transfer \\ -V_{millipede}(t - \phi_t) & propulsive \end{cases} \tag{2.6}$$

$$y(t) = \begin{cases} H - R - R\cos(\omega(t - \phi_t)) & transfer \\ 0 & propulsive \end{cases} \tag{2.7}$$

In these generalized position equations, the time phase between adjacent legs is $\phi_t = \frac{d}{V_{wave}}$. The relationship between the period of the transfer state(t_t) and the period of the propulsive state(t_p) determines most of the characteristics of the system once the radius for the reference circle is determined. This relationship is called the duty cycle:

$$D = \frac{t_t}{t_p} \tag{2.8}$$

Figure 2.3: Duty Cycle

2.1.2 Qualitative Understanding of Metachronal Gait

The traveling wave phenomenon of the Myriapoda is a central aspect of its locomotion. The Myriapoda modulates the wave propagating through its legs to produce thrust or speed. Garcia et al. [5] showed that the metachronal gait specific to millipedes makes them highly capable of burrowing. Garcia's analysis of the millipedes metachronal gait found that the duty cycle ranges between 0.3 to 0.7. The lower duty cycle gait creates greater velocities for the millipede, in contrast to the higher duty cycle gait that produces greater thrust and lower speed.

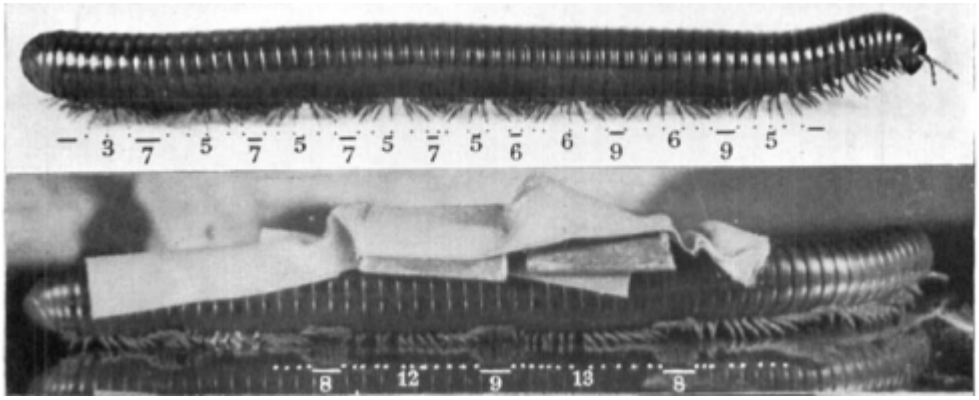

Figure 2.4: From [12], The Millipede adjusts the number of legs in a 'backstroke' and 'forestroke' according to torque needs. Numbers compare legs in propulsive and transfer state, i.e. backstroke and forestroke. Greater number of legs in propulsive state, the greater the thrust is generated.

Fig. 2.4 shows the metachronal wave's effect on torque, improving its ability to carry a payload. Research by Kano et al. [9] also studied the metachronal wave characteristics of the millipede, focusing on the millipede bio-sensory feedback systems.

Chapter 3

Design

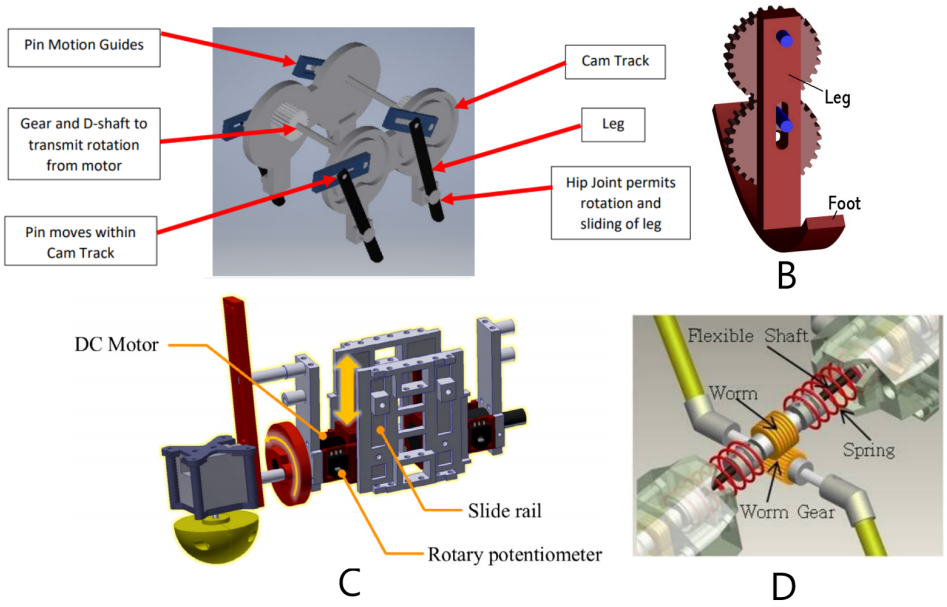

Figure 3.1: Existing leg designs within the academic literature. From (A) Garcia's[7] inspired cam design, (B) Long's[11] gear bar mechanism; behaves much like a 4-bar mechanism, (C) Kano et al. [9] leg device with closed feedback system, (D) Koh et al. [10] single motor fixed rotary leg. Analysis covers (B) and (A), but observed (C) and (D) for characteristic inspiration

The broad design goal of Walker is to create a straightforward simplified omnipede robot. Due to the limitations driven by the COVID 19 pandemic, research avoided development beyond parts other than leg mechanisms. This chapter is dedicated entirely to researching leg mechanisms as a basis for the Walker robot build and simulation.

3.1 Legs

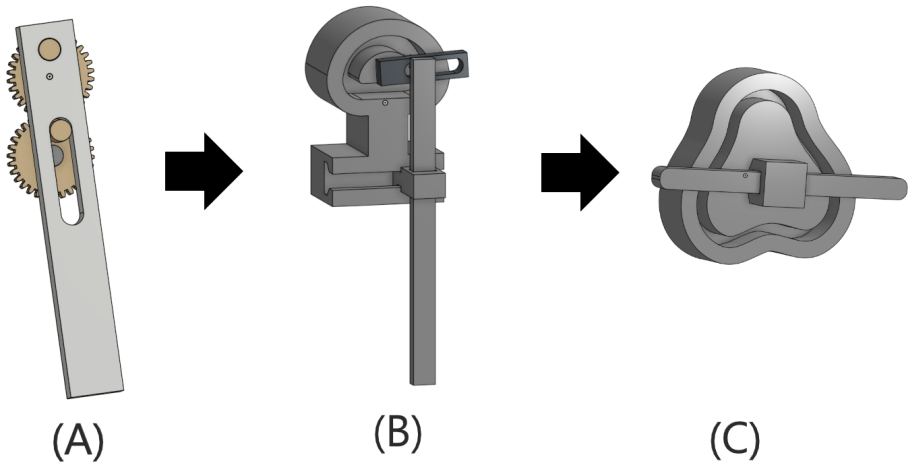

Figure 3.2: The evolution of leg designs, beginning with (A) a two gear system based on fig 3.1B, (B) my own cam/shaft design inspired by 3.1A, and (C) implementation of the cam suggested by Wan and Song [19]

Determining a leg actuation device is a primary consideration of this paper. To create a simple millipede-like robot, a novel and reproducible leg is necessary. In this chapter, existing leg actuators in the academic literature are analyzed, improved upon, and 3D modeled in Fusion 360 for manufacturing analysis. After analysis of two actuators, the novel cam mechanism suggested by Wan and Song [19] was determined to be the best device for Walker.

The design goals of the leg actuator are as follows:

- A single actuated leg with one degree of freedom
- Minimized individual parts to less than three
- Path of the foot creates a half-circle trajectory described in Section 2.1

The scoring rubric compares the number of parts, whether the device creates the desired trajectory, and a non-rigorous fault score for any additional issues with the design to systematically determine the best leg mechanism. The number of parts garners a score of five if less than three and subtracts one point for each additional part. The desired trajectory gives a flat score of five if met and zero if not. Overall the categories are added and subtracted by the fault score.

Determining the leg actuator that accomplishes these design goals begins with reviewing existing millipede robot leg mechanisms. The designs shown in Fig. 3.2 are the basis of the review. The Kano et al. [9] design, seen in Fig. 3.1(C), is too complex for the purposes of my research. Kano's research focused on control theory actuation over design simplicity. The design by Koh et al. [10], element Fig. 3.1(D), focused on design simplicity of a millipede robot using fixed rigid legs. However, the Koh design features little gait modulation.

The investigation begins between the complexity of the Kano et al. [9] design and the simplicity of the Koh et al. [10] design, with the design of Long et al. [11] seen in Fig. 3.1(B). This design met the requirement of a single rotating actuator and few parts.

3.1.1 Modeling Geared Bar Mechanism

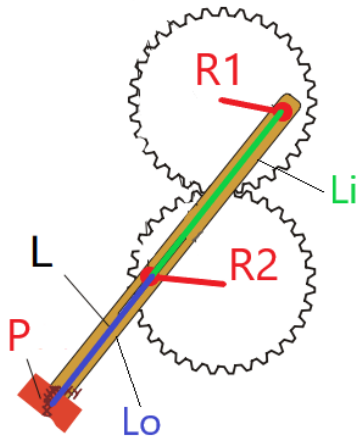

Figure 3.3: Derived from [11], Diagram of the geared bar actuator

The first mechanism is derived from Long et al. [11] i.e Fig. 3.1(B). The device has similarities to 4-link and 5-link drive mechanisms. The benefit of this construction is its simple two gear, single motor design.

$$\vec{C_1} = \begin{pmatrix} R_1 \cos(\theta(t)) \\ R_1 \sin(\theta(t)) \end{pmatrix} \tag{3.1}$$

$$\vec{C_2} = \begin{pmatrix} -R_2 \cos(\theta(t)) \\ R_2 \sin(\theta(t)) - (R_1 + R_2 + 2d) \end{pmatrix} \tag{3.2}$$

$$\begin{aligned} \vec{L_i} &= \vec{C_2} - \vec{C_1}; \\ \hat{L_i} &= \frac{\vec{L_i}}{|\vec{L_i}|} \end{aligned} \tag{3.3}$$

$$\vec{P} = (L - |\vec{L_i}|)\hat{L_i} + \vec{C_2} \tag{3.4}$$

Assuming a constant angular velocity ω, the angular position of the drive gear is $\theta(t) = \omega t$. Each gear has a peg distance d away from the gear's radius. The position of the pegs on an XY-plane are referred to as C_1 and C_2 respective to the gears of R_1 and R_2. The length of the leg is L. The equations below derive the position of the leg $\vec{P}$ in two-dimensional vector form.

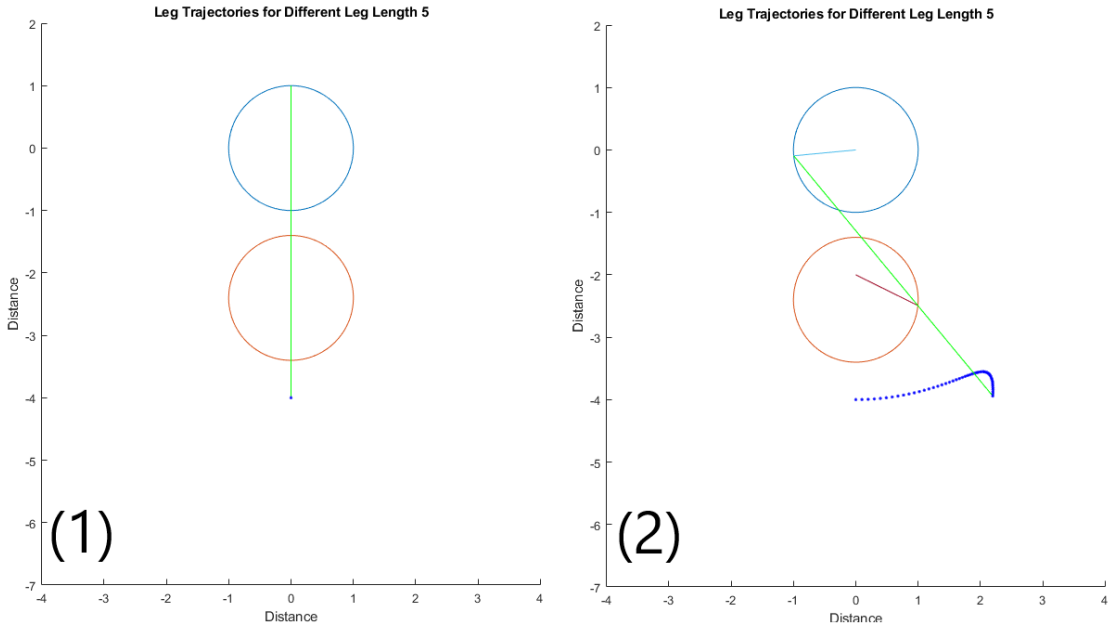

Figure 3.4: Trajectory of geared bar mechanism with L = 5 from kinematic equation 3.4

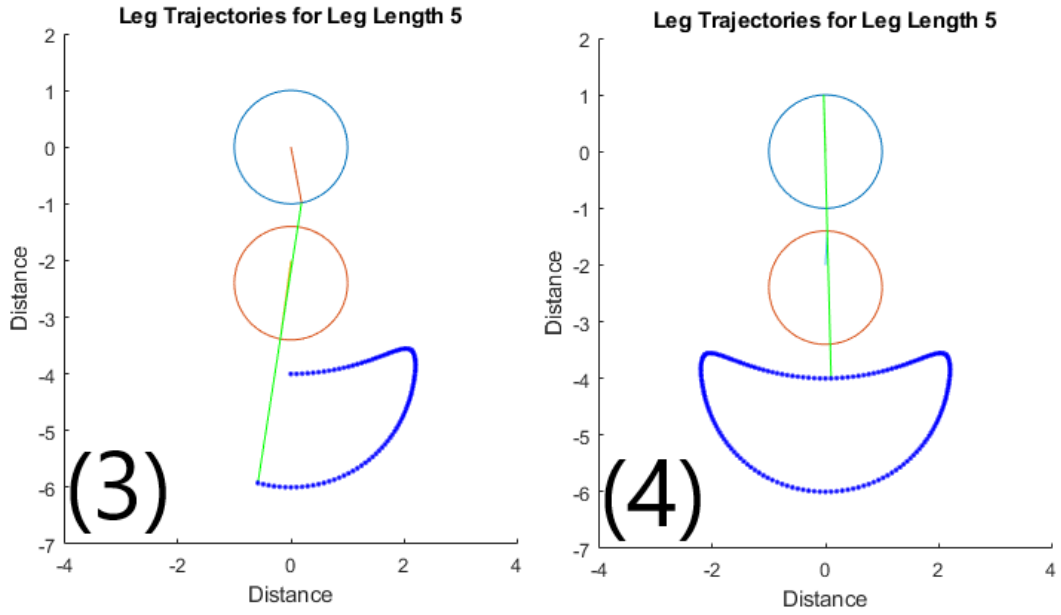

Figure 3.5: Trajectory of geared bar mechanism with L = 5 from kinematic equation 3.4

With this relationship between output $\vec{P}$ (the travelling path of the foot) and input $\theta(t) = \omega t$, path analysis can occur where the leg length is arbitrarily set to 5 (see Fig. 3.4). The trajectory acquired is not the desired half-circle path that the

kinematic model defines. Any analysis beyond changing the length of the leg is beyond the scope of this project. Leaving the gear ratios static, i.e. $R_1 = R_2$, leg lengths affect the trajectory of the mechanism as shown in Fig. 3.7.

The short analysis shown in Fig. 3.7 determined that a longer the leg length results in a flatter curve of the propulsive state. The shape still doesn't meet the desired trajectory. In summation, the gear mechanism doesn't have the desired trajectory but does have a simple design with few parts. An additional concern is the difficulty of printing gears. All parts manufactured were 3D printed, restricting printing contours smaller than .5mm, greatly reducing the number of teeth these gears can possess. For this reason, the fault score is -2 points. **This gear mechanism doesn't meet the requirement of a half-circle trajectory (see Fig. 2.1), though it is a single motor system.**

Table 3.1: Leg Actuation Score Matrix

Design	Parts	Desired Trajectory	Faults	Overall
Gear Mechanism[11]	3	No	-2	3/10

The mechanism is also designed and assembled in Fusion 360 (see Fig. 3.6) for testing of motion and manufacturing feasibility. Fig. 3.8 shows snapshots of 90 degree out of phase motion of the mechanism.

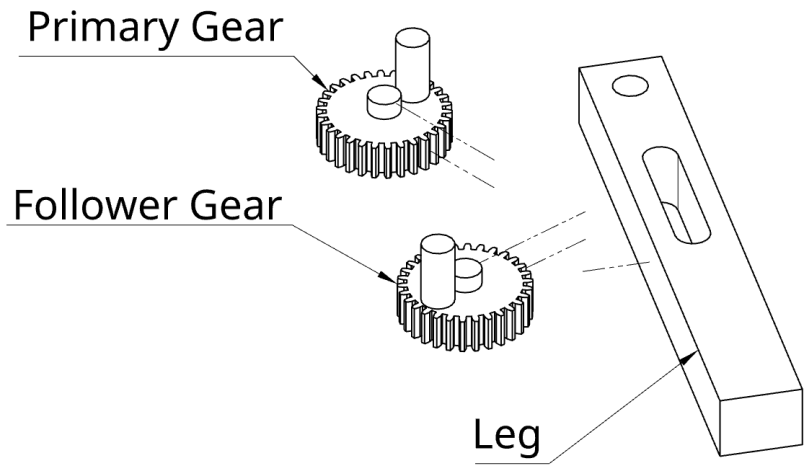

Figure 3.6: Fusion 360 3D modeled gear bar leg mechanism parts

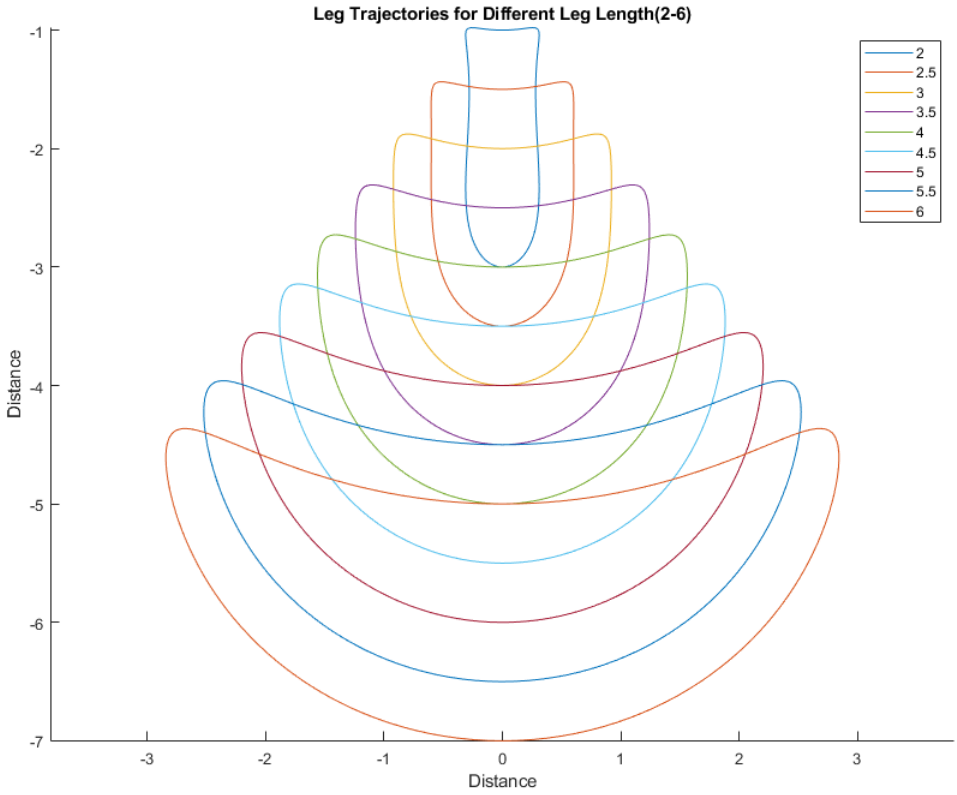

Figure 3.7: Geared bar trajectories from different leg lengths determined from kinematic equation 3.4

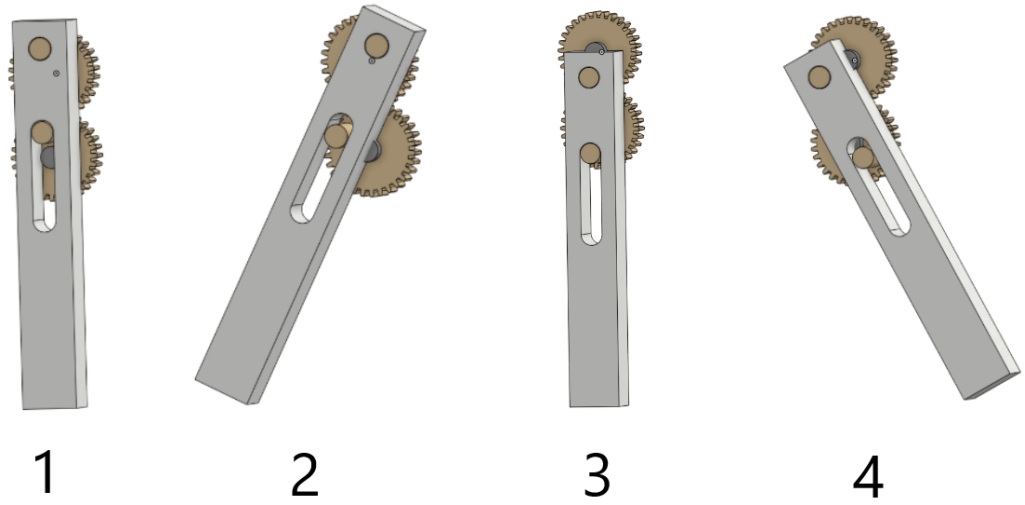

Figure 3.8: Motion of Fusion 360 assembled geared leg mechanism based on [11]

3.1.2 Modeling Cam Design

Garcia et al. [5] derives a cam actuator based on the design suggested by Wan and Song [19]. The paper by Wan and Song derives a leg device based upon custom cam curves for developing desired trajectories, defining a cam shape that creates a half-circle trajectory. This cam design was also investigated by Crow [3] in a mechanical engineering dissertation. The Garcia [7] design shown in Fig. 3.1(A) modifies the Wan and Song [19] design in favor of a single rotating leg, while the Crow [3] design follows the original actuator more closely. Fig. 3.9 shows the original cam design. Due to the complexity of the cam shape, I developed an original mechanism inspired by Garcia [7]'s design, though this was not used in the final design.

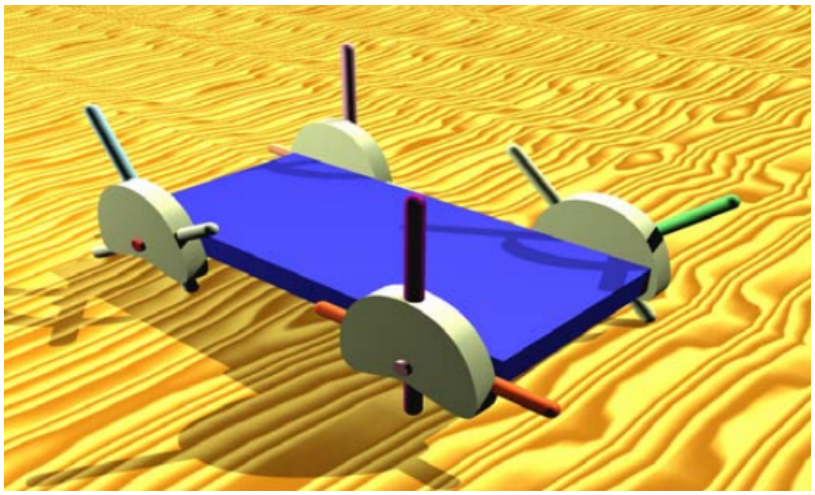

Figure 3.9: Source cam design from Wan and Song [19]

3.1.2.1 Custom Cam Design

Seen in Fig. 3.2(B), this device was developed myself. The mechanism is an intuitive design that translates the trajectory path of the inner cam shape down by the length of the leg. The shape of the cam is the exact trajectory of the foot, translated by the length of the leg. The device can support a leg of any length, and a cam of any shape, given that there is low jerk, i.e., no curves too sharp on the cam shape, making it exceptionally intuitive to get the desired trajectory without much calculation.

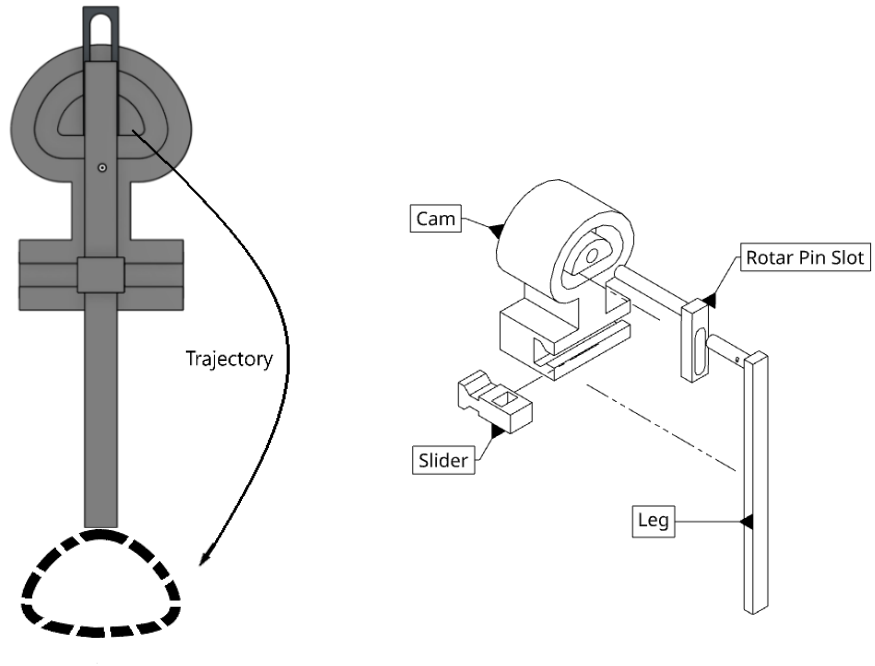

Figure 3.10: Fusion 360 3D model of custom sliding leg cam design

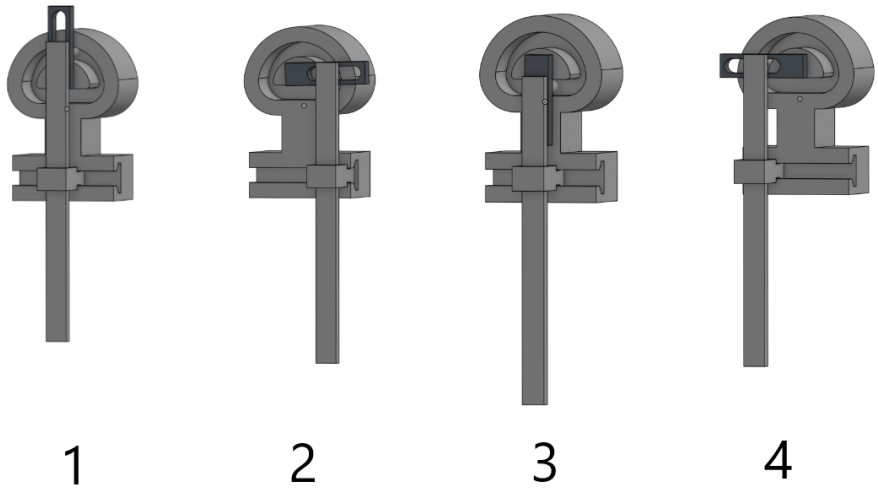

Figure 3.11: Fusion 360 assembly, custom sliding leg cam motion

The pitfalls of this design include the many parts and a large number of friction points. The sliding joint and the peg that fit into the cam shape are two major points of friction. Secondly, a large amount of torque is pressed on the pin slot if the

interior cam shape is too narrow. These combined factors lead to a fault score of -3. **Due to the limiting factors including the friction and the amount of parts, other actuation devices are investigated.**

Table 3.2: Leg Actuation Score Matrix

Design	Parts	Desired Trajectory	Faults	Overall
Gear Mechanism[11]	3	No	-2	3/10
Slide Cam Mechanism	4	Yes	-3	6/10

3.1.2.2 Original Fixed Bearing Distance Design

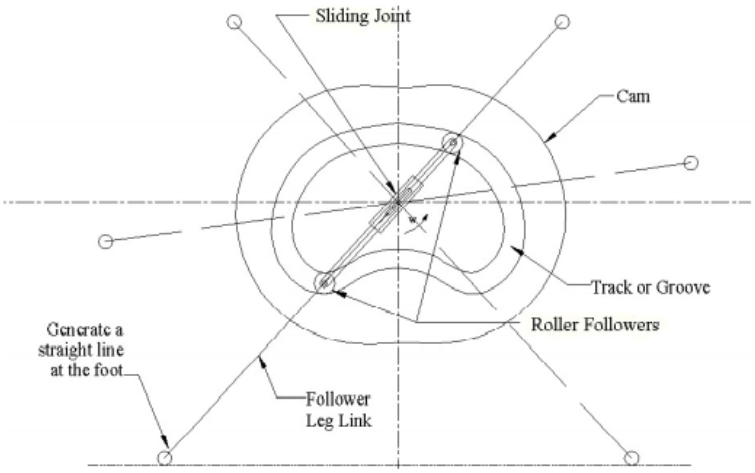

Figure 3.12: Extended leg follower and closed form cam from [19]

The third and final mechanism is the most closely related implementation of the cam design from the paper by Wan and Song [19]. This design was also the leg device used in the final build of Walker.

The kinematic equations of motion that describe the half circle trajectory define the shape of the cam profile. The assembly of the mechanism is displayed in Fig. 3.12 which includes a rotating link with bearings at a fixed difference and a sliding joint with a leg link attached. Fig. 3.13 defines the variables to be determined in the upcoming analysis, also defined here:

- L = length of leg

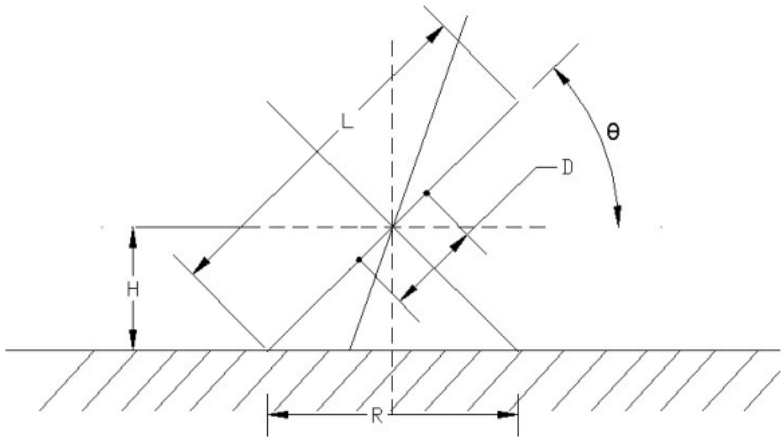

Figure 3.13: Variables of cam design from Wan and Song [19]

- d = distance between bearings
- H = height from straight line trajectory
- θ = Angle of rotation of bearing link

The cam shape maintains a constant width d through rotation and is symmetrical about the Y axis. Consequentially, a single function($f(\theta)$) describing the shape of the curve from $(0°, 90°)$ will define the entirety of the cam shape as prescribed in Equations 3.5-3.8. Refer to Wan and Song [19] for further description.

$$S_1 = f(\theta), 0° < \theta \leq 90° \tag{3.5}$$

$$S_2 = f(\pi - \theta), 90° < \theta \leq 180° \tag{3.6}$$

$$S_3 = d - f(\theta - \pi), 180° < \theta \leq 270° \tag{3.7}$$

$$S_4 = d - f(2\pi - \theta), 270° < \theta \leq 360° \tag{3.8}$$

Represented in polar coordinates, an angle value represents the rotational position of the central rotating arm. The entire upper half of the cam curve should create a straight line trajectory for the bottom half of the half circle trajectory. The height of the leg is -H at every point in this function. Hence, R will be dependent on θ.

$$\begin{aligned} Y &= -H \\ R\sin\theta &= -H \\ R &= \frac{-H}{\sin\theta} \end{aligned} \tag{3.9}$$

As laid out by Wan and Song [19] in the original paper, this cam will equally segment a leg when in a vertical position. So the max height of the function is known at angle $\theta = 90°$. The function describing the first quadrant is then:

$$S_1 = f(\theta) = R = \frac{L+d}{2} - \frac{H}{\sin(\theta)} \tag{3.10}$$

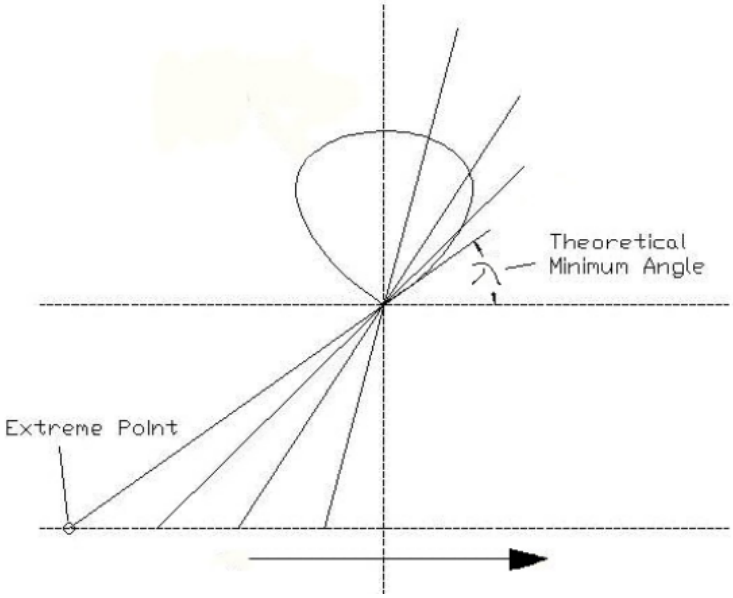

Figure 3.14: Cam trajectory from Wan and Song [19]

When the leg link becomes tangential to the cam curve in the first quadrant, the relationship of Equation 3.10 will go to negative infinity as θ becomes small. The minimum theoretical angle is the angle at which the radius of the cam curve = 0.

$$\begin{aligned} R = 0 = \frac{L+d}{2} - \frac{H}{\sin(\theta)} \\ \frac{L+d}{2} = \frac{H}{\sin(\theta)} \\ \theta = \lambda = \arcsin\frac{2H}{L+d} \end{aligned} \tag{3.11}$$

Angles less than λ are invalid, but the above equation defines the radius of the curve for all angles greater than λ. The value of λ determines the span (length of flat trajectory) that the leg makes a straight-line trajectory. The goal is to choose values for axle height H, leg length L, and bearing width d to maximize the straight-line trajectory span. The value of λ is defined by Equation 3.11.

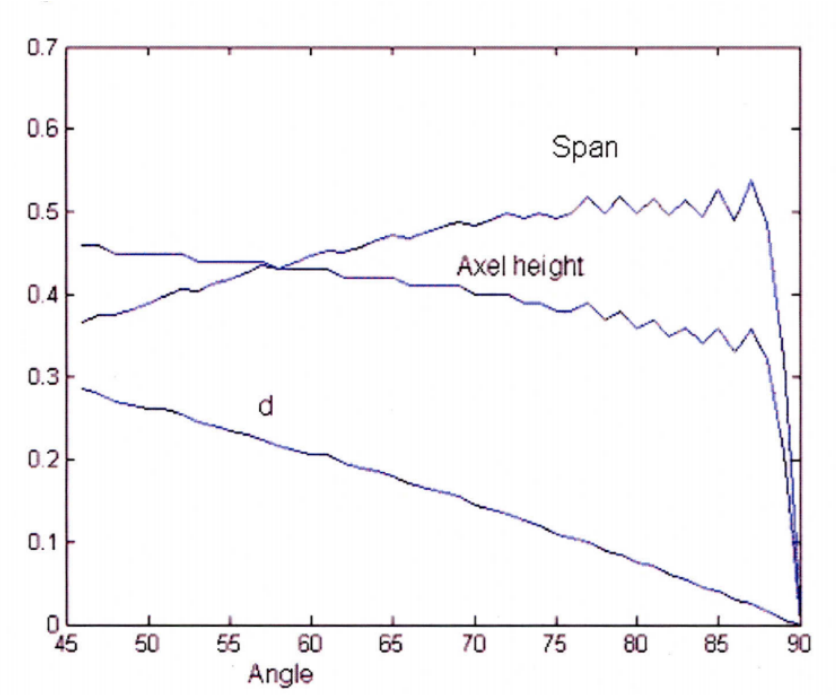

Figure 3.15: Angular span vs. d/L, H/L, and X_{gait}/L from Crow [3]

Values for H, d and L must be selected to further define the shape. The paper by Crow [3] compares the relationship between the span of the leg stroke and the values for H, d and L in Fig. 3.15. Crow [3] finds that choosing an angular span of 60° maximizes the axle height H, bearing width d, and span, also subdividing the mechanism into six equal rotational segments. With an angular span of 60°, the cam parameters are shown below, which create the shape shown in Fig. 3.16:

- H = .43L
- d = .195L

A curve must smoothly connect the upper portion of the cam profile to the lower part. The variable α defines an angle arbitrarily greater than λ as a smoother connection point than λ, from which would be impossible to create a smooth curve. Iterative testing for smooth cam curves determines α.

To find a function that defines the shape of the cam curve from $0° < \theta \leq \alpha$ requires polynomial fitting or polynomial spline interpolation, also known as spline interpolation. Wan and Song [19] suggests a sixth-order polynomial to describe this

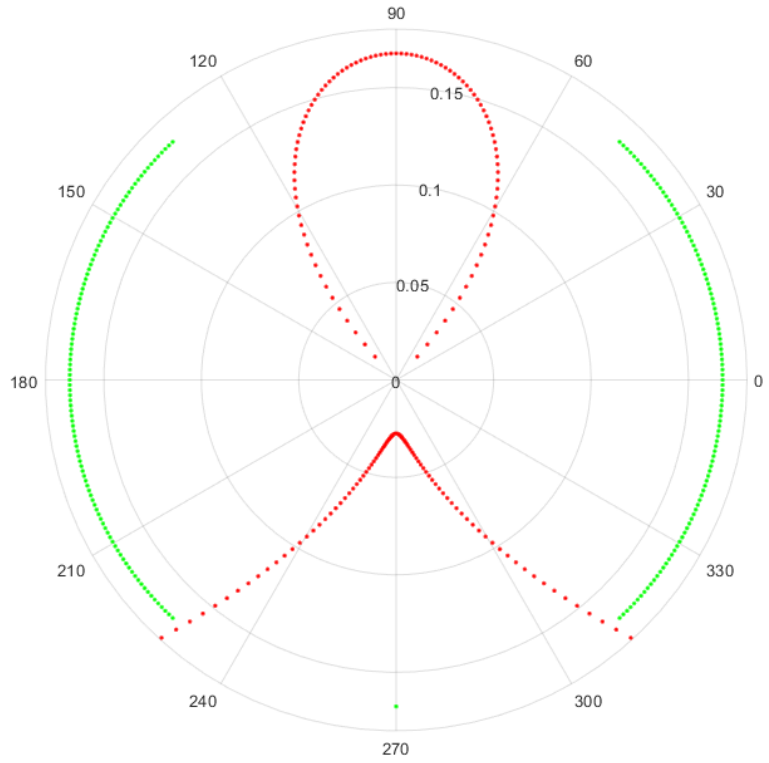

Figure 3.16: Cam shape excluding angles below the theoretical minimum, H=.43L, d=.195L

curve, and Crow [3] uses a fourth-order polynomial. Both of these methods are far beyond the scope of this paper but refer to Conte and De Boor [2][4] for inspiration on polynomial approximations and interpolation. The cam curve between 0 and α is determined using Matlab functions for interpolation. See Fig. 3.17 for the outcome of different interpolation methods.

In these initial curve fittings the shape is far to sharp at $\theta = 90^\circ$ i.e. the bottom and top of the cam curve. To reduce this jerk motion, a wider diameter is used at an arbitrarily selected value of $d = .4$, determined through trial and error. The curve is then shown in Fig. 3.18.

Crow [3] departs from the original 2004 cam design. His axle height and bearing width values were a point of reference, but further analysis determined that these values were incorrect for my build. In place of Crow's original variable values, approximations through iterative analysis on Matlab yielded values used below.

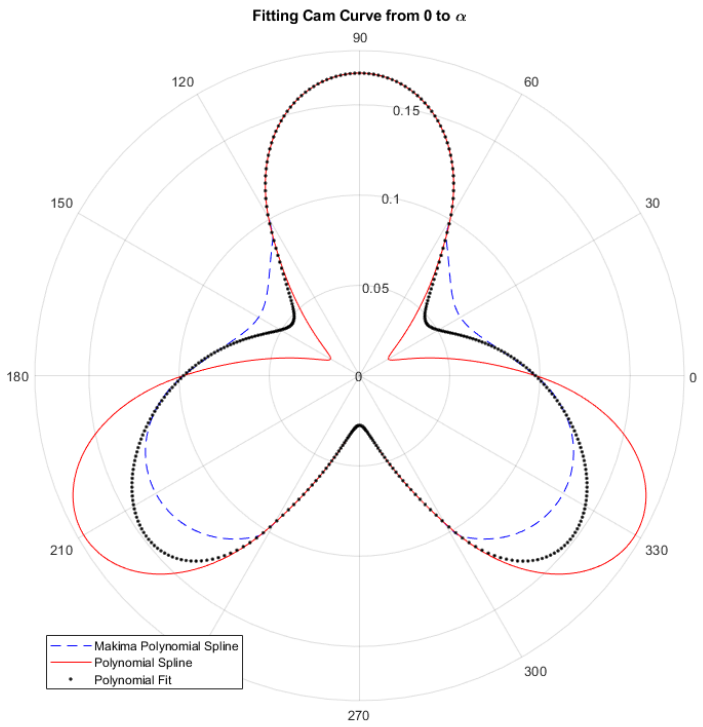

Figure 3.17: Cam shape with interpolation between 0 and α H=.43L, d=.195L

Two of the most desirable cam shapes are shown in Fig. 3.19 and Fig. 3.20. The shapes maximize axle height for greater foot clearance height while reducing sharp curves.

The "Makima Polynomial Spline" in Fig. 3.20 is the shape used in the final build. Unlike the original proposed shape, the final design removes the exterior follower wall in favor of a single interior cam shape with a rotating armature. See Fig. 3.21 for visual representation. **With this final design, I conclude the investigation of leg devices. The mechanism creates the desired half-circle foot trajectory, the number of separate parts is 3 (the pegs are considered part of the leg), overall friction is decreased, and the parts are large enough that print resolution can be coarse ($> .5mm$).** The mechanism's only fault is the torque forces that will occur on the leg when nearing the vertical position. This fault garners a fault score of -1, as all other design flaws are insignificant compared to the previous two devices.

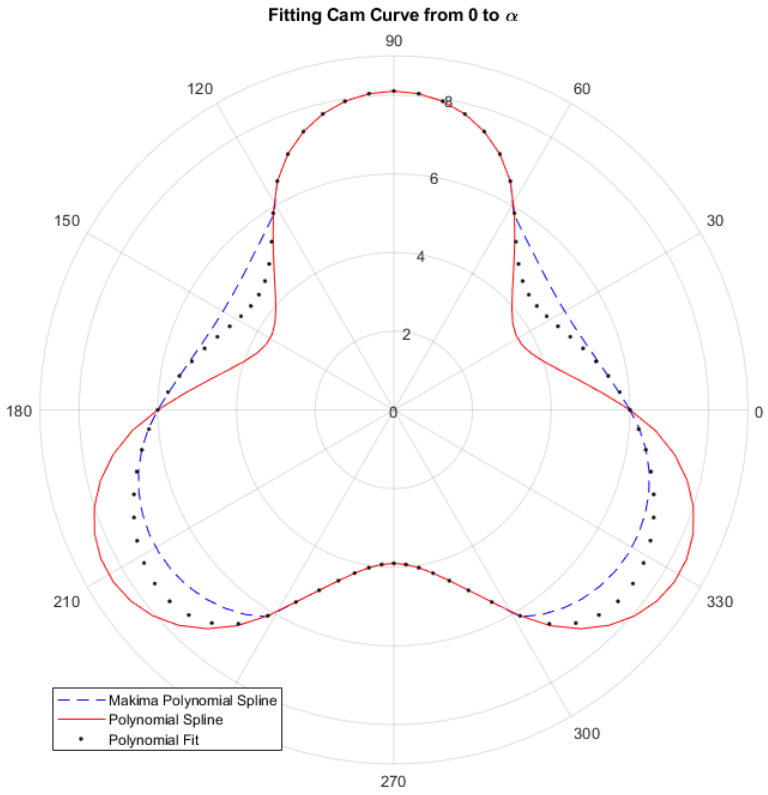

Figure 3.18: Cam shape with interpolation between 0 and α, d=.4, H=.43L

3.2 Conclusion

Fig. 3.2 shows the evolution of leg designs. Walker's leg is determined after implementation of Fig. 3.2(A) Long's[11] barred gear leg mechanism, creation of my own intuitive "slide cam mechanism" Fig. 3.2)(B), and analysis of the novel cam design by Wan and Song [19] Fig. 3.2)(C). The final 3D model suggested by Wan and Song [19], shown Fig. 3.21, is robust yet straightforward. Table 3.3 shows a scoring matrix. The next chapter simulates the leg device, followed by a 3D print in the following chapter.

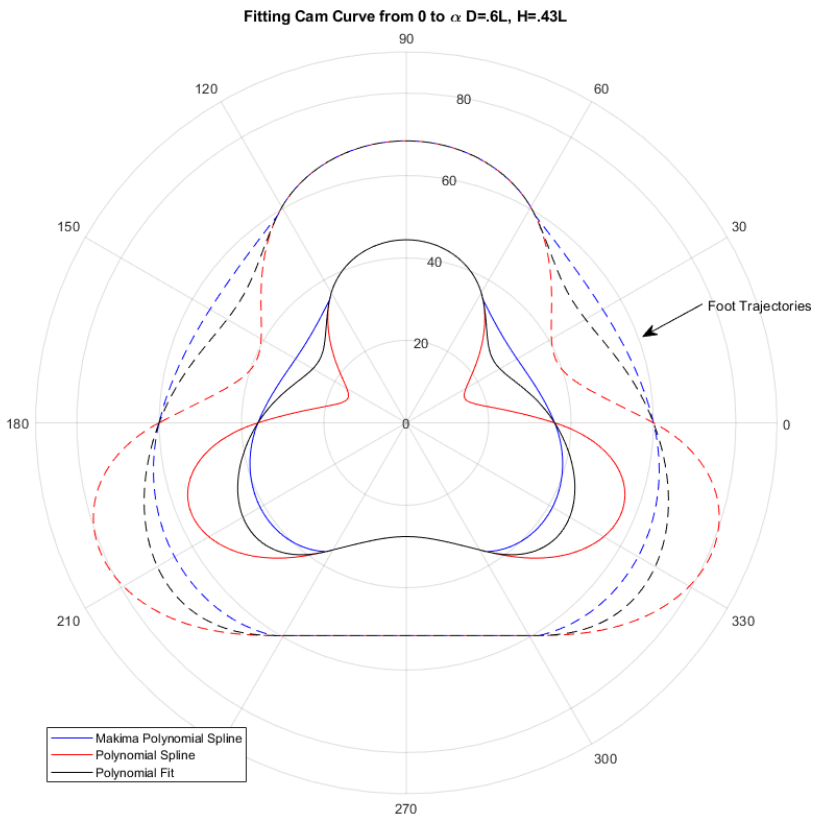

Figure 3.19: Full cam shape with polynomial spline, d=.6L H=.43L

Table 3.3: Leg actuator score matrix

Design	Parts	Desired Trajectory	Faults	Overall
Gear Mechanism[11]	3	No	-2	5/10
Slide Cam Mechanism	4	Yes	-3	6/10
Regular Cam Mechanism[19]	3	Yes	-1	9/10

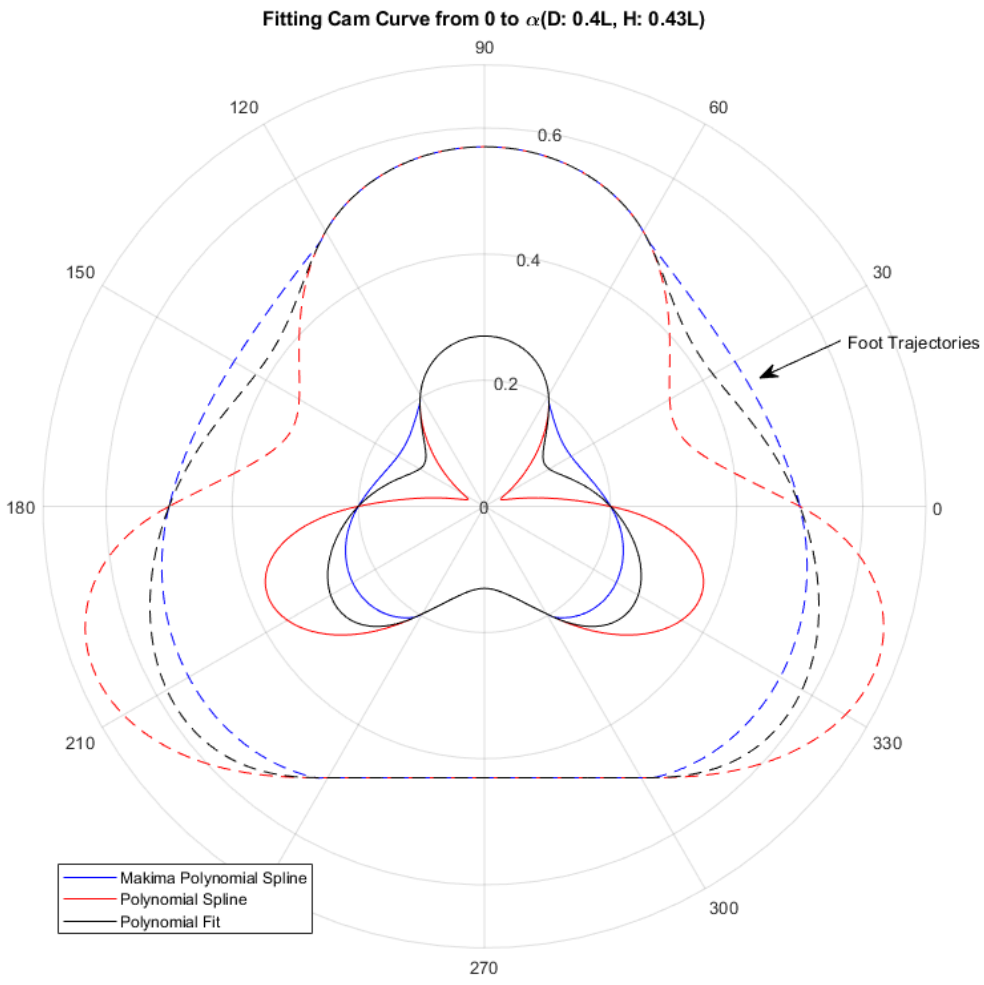

Figure 3.20: Full cam shape with polynomial spline, d=.4L H=.43L

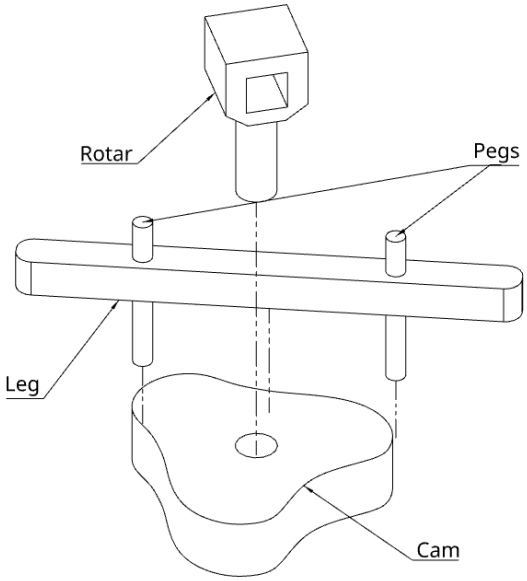

Figure 3.21: Wan and Song [19] cam design, modeled in Fusion 360

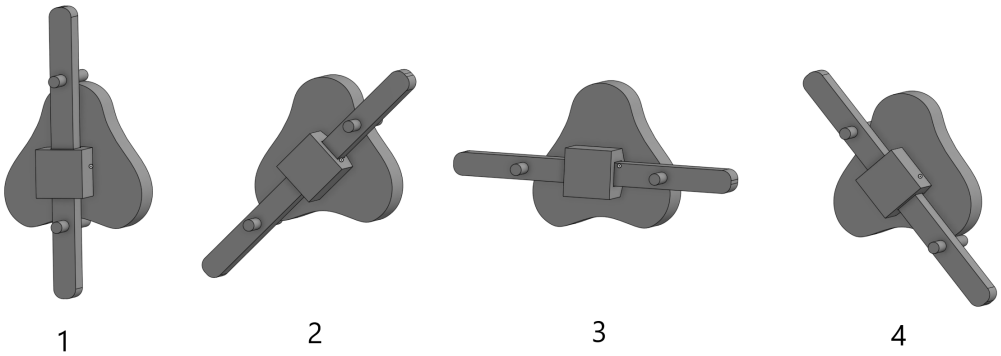

Figure 3.22: Wan and Song [19] cam design, Fusion 360 assembly. Snapshot of motion

Chapter 4

Simulation

In this chapter, a Matlab Simscape Multibody simulation models the chosen cam design shown in Fig. 3.21. Prior to the dynamics analysis of the 3D simulation environment, Section 4.1 shows the analysis of the kinematics defined in Section 2.1.1. This chapter strays from simply mimicking millipede motion and focuses on maximizing the stability of the robot design based upon the developed cam actuator.

Section 1.3 discusses the thrust advantages to a millipede-like motion. Garcia's[7] study of millipede locomotion further explores the thrust benefits. My analysis recognizes these benefits but focuses on the stability of the Myriapoda motion rather than speed or thrust potential. An understanding of the stability of my system proves its efficacy, which future studies can then modulate for a specific analysis of insect gaits.

4.1 Kinematic Equation Analysis

This section conducts an initial motion analysis, utilizing the kinematic equations derived in Section 2.1.1. Fig. 4.1 shows the trajectory of a single foot of a millipede as defined in the paper by Sathirapongsasuti et al. [18] discussed in Section 2.1.1. The rotating leg that creates wave-like motion through the legs of a millipede individually draws out a cycloid viewed from a static world frame. The analysis in this section will be concerned with maximizing foot contact with the ground during forward motion. The goal is to find a gait pattern that maintains at least one foot in contact with the ground at all times. The number of legs, the phase difference between each leg, and millipede or centipede-like motion define the

different gait (see Fig. 1.1). The following section conducts stability analysis in the 3D Simscape environment, but a kinematic equation analysis narrows the viable, stable gait patterns. In addition, the Simscape environment takes upwards of fifteen minutes per simulation to compile and run. As mentioned above, Fig. 4.1 displays a

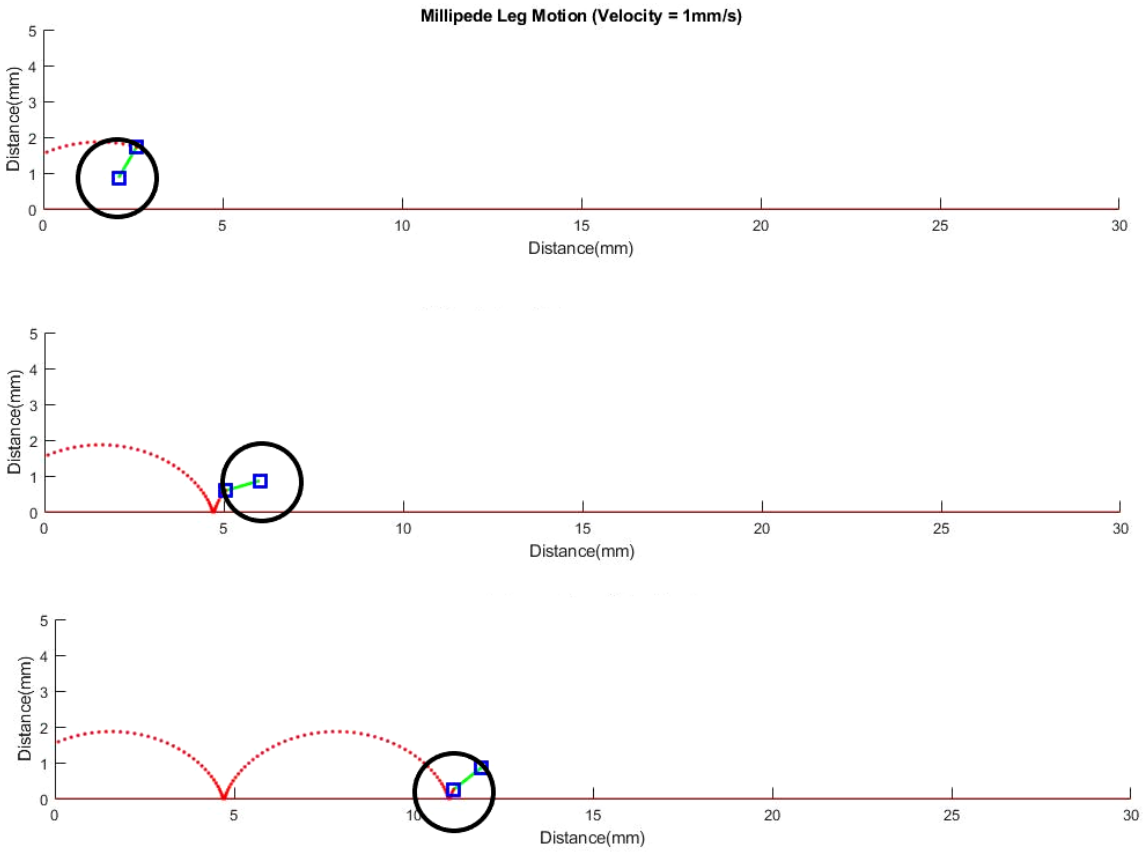

Figure 4.1: Initial stability analysis expands upon single cycloid created by travelling leg, shown in Section 2.1.2. We want to maximize amount of time that the leg is in contact with the ground.

snapshot of a single rotating leg in motion and the path it draws. The cam actuator developed in Section 3.1.2.2 is two-sided, meaning that each leg device draws out two of these cycloids, 180 degrees out of phase with each other. Building on the single rotating leg, multiple two-sided legs in motion are studied as shown in Fig. 4.2 (a snapshot of the movement of the legs), to model the final robot design.

Table 4.1 compares each gait pattern's effect on contact with the ground. Across the board, the centipede-like motion reduces the time there is no ground contact.

For the Walker robot, this creates more significant stability with fewer legs, lowering the cost of the robot. With this cursory survey of equilibrium and motion, Section 4.2 discusses developing the 3D simulation environment in Matlab Simscape Multibody.

Leg Pairs	Phase Difference (deg)	Millipede-like Time(sec)	Centipede-like Time(sec)
2	0	3.14	1.56
2	30	2.1	0
2	60	1.05	0
2	90	1.56	1.56
3	0	3.14	1.56
3	30	1.05	0
3	60	0	0
3	90	1.56	1.56
4	0	3.14	1.56
4	30	0.52	0
4	60	0	0
4	90	1.56	1.56
5	0	3.14	1.56
5	30	0	0
5	60	0	0
5	90	1.56	1.56
6	0	3.14	1.56
6	30	0	0
6	60	0	0
6	90	1.56	1.56

Table 4.1: Period in which each gait has no contact with the ground

4.2 Simscape Multibody Simulations

Simscape Multibody is part of the Mathworks toolkit and is the primary source of testing for this paper. Section 4.2.1 covers the iterative simulation design process followed by an overview of the final simulation in Section 4.2.2 and some preliminary data before comparison with the experimental data of Ch. 5.

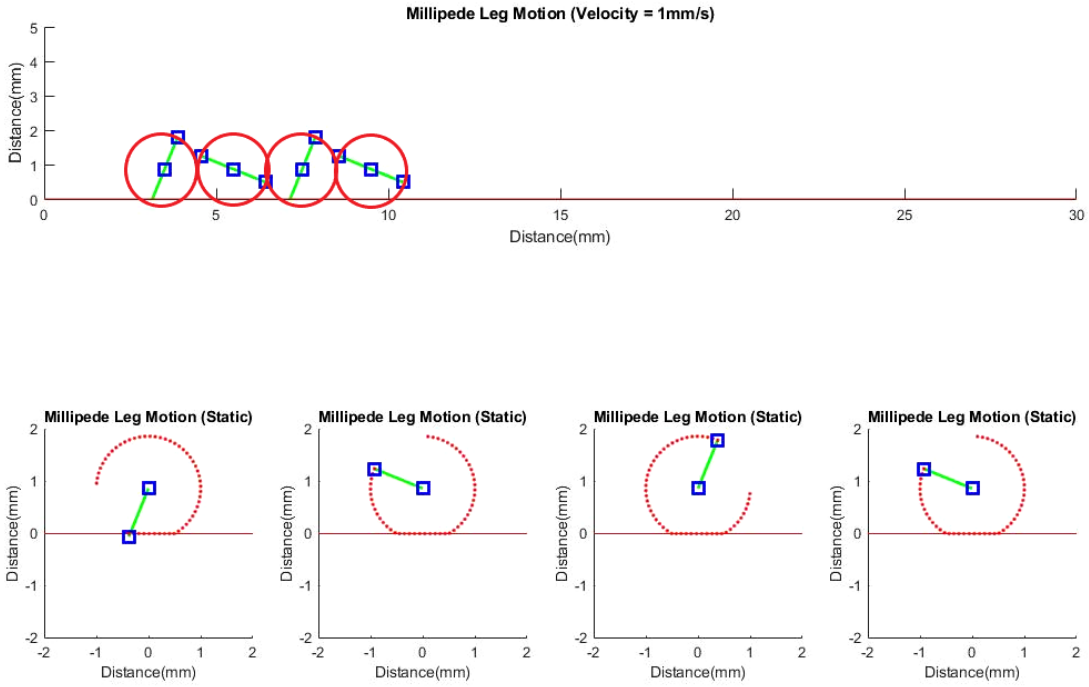

Figure 4.2: Snapshot of Matlab motion video. Video displays the system moving forward when leg is in contact with ground. Number of legs and phase difference between legs effect on position expands upon single cycloid. Analysis shows that centipede motion creates greater stability with fewer legs.

4.2.1 Iterations of Simulation Environment

The simulation environment changed significantly throughout the course of the project. Fig. 4.3 shows the several stages of development. The 1st generation Simscape environment provided an extremely rough conceptual image of the desired end prototype without any conception of the leg actuator to be used for the robot. My research of gait dynamics primarily used the 1st generation environment to develop familiarity with Simscape Multibody and develop a general structure for the development environment. The development process with Simscape involved uploading the Fusion 360 bodies to Onshape.com and creating joint assemblies uploaded to Matlab.

The second-generation simulation implemented the custom cam mechanism discussed in Section 3.1.2.1 and some custom-made body segments. Simulating a rotating arm pushing the leg around an enclosed cam shape proved challenging.

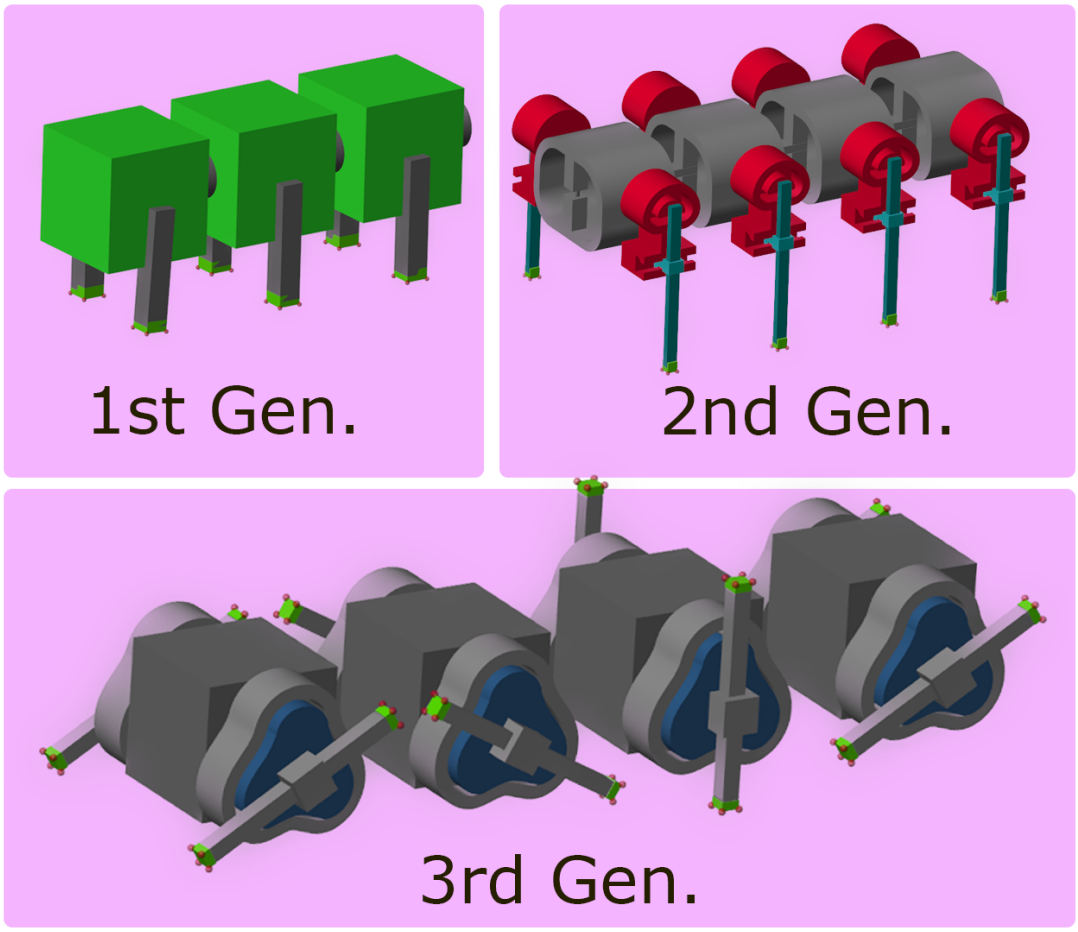

Figure 4.3: Generations of design. First design is an extremely rough proof of concept. Generation two attempted to use custom cam design made myself that proved too complex to simulate. Third and final generation is simpler than second, reducing body to plastic block, and using novel cam actuation device.

The design removed the rotating component and simulated the motion without that contact point, resulting in an inaccurate simulation that was not representative of the leg design. My research of dynamics abandoned the second-generation environment for these reasons as well as those discussed in Chapter 3.

The third generation simulation, the complete environment, simplified the body design and used the fixed bearing cam actuator, discussed further in Section 4.2.2.

4.2.2 Final Simscape Environment

The third generation Simscape environment, the final result, is pictured in Fig. 4.5, with the component body segment subsystem shown in Fig. 4.4, and the component leg subsystem shown in Fig. 4.6. The primary focus of the environment is to provide an accurate analytical tool for gait dynamics and prove the efficacy of the developed cam actuation device. Unlike the second-generation model, this final environment accurately simulates the leg trajectory. Though features of the robot such as exact body shape and center of gravity are not included, they are trivial to add in future work. The lack of physical modeling of the connections and body had a negligible effect on studying the stability of the systems gait dynamics.

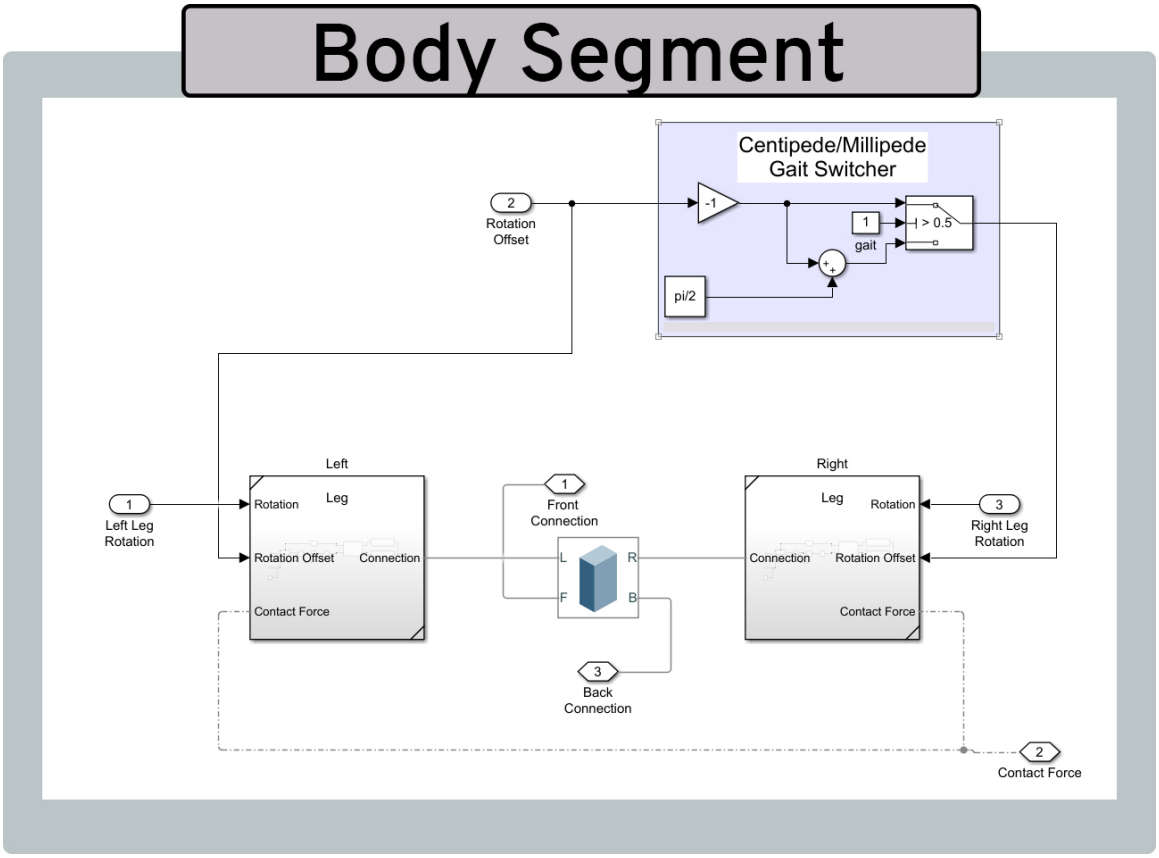

Figure 4.4: Snapshot of a single body segment component from Simscape environment. All body segments a are duplicate of this one. Rotation of the leg is controlled by angular position values. The gait switcher adds simple user interphase for changing left and right leg ninety degrees out-of-phase.

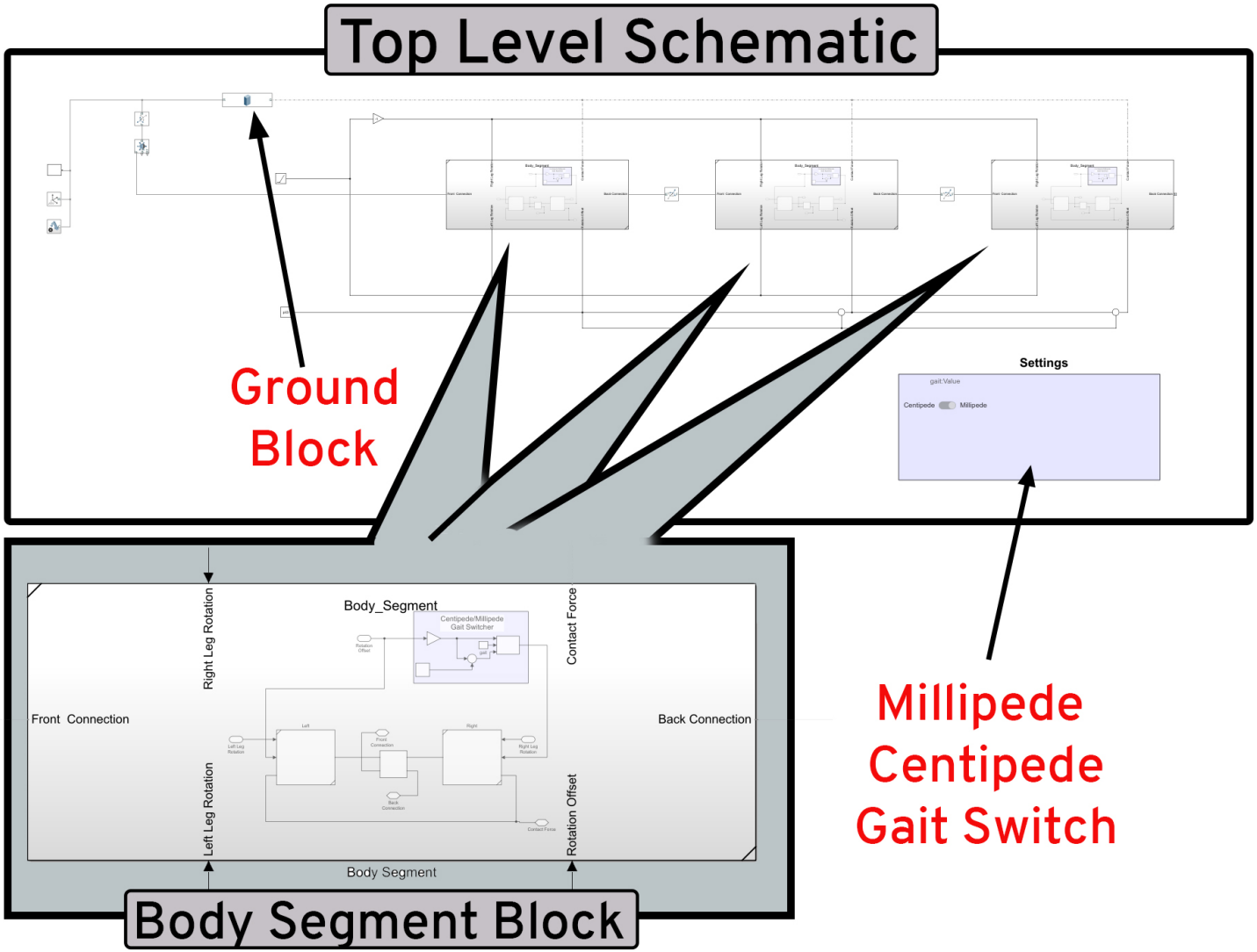

Figure 4.5: Snapshot of Simscape simulation environment

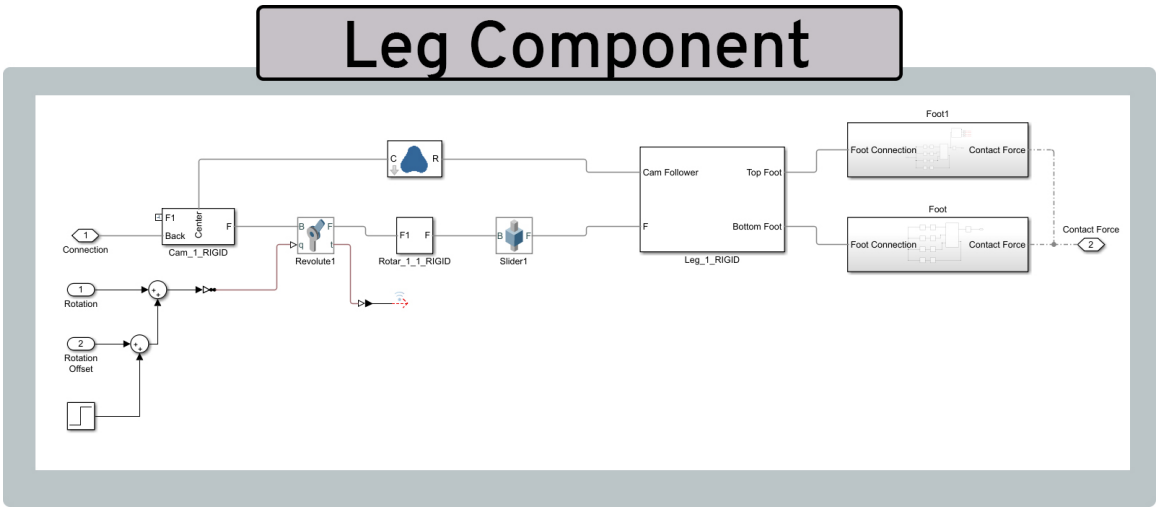

Figure 4.6: Snapshot of leg segment component from Simscape environment, contained within the body segment component. A revolute joint and slider control the rotating arm constrained by a cam shape. A foot is attached to either side of the leg with four contact points for measuring ground contact.

4.3 Simulation Results and Conclusion

Preliminary kinematics analysis yielded the data in Table 4.1, suggesting that the centipede system is more stable across the board if stability is primitively defined as maintaining leg contact with the ground. Furthermore, the centipede gait with a phase difference of 60 degrees between neighboring legs provides the most ground contact overall. With the final Simscape environment developed, a ten-second simulation is run on flat terrain to measure the cross-sectional center of gravity from the different gait patterns researched in Section 4.1.

Fig. 4.8 shows the results of comparing four different gait patterns with 60 deg phase difference and a variable number of legs. The centipede gait causes extreme vertical instability but excellent horizontal stability. The centipede motion tends towards more chaotic swaying as well as drift but within a confined region. Of the tested locomotive patterns, the centipede motion with eight legs is the most stable.

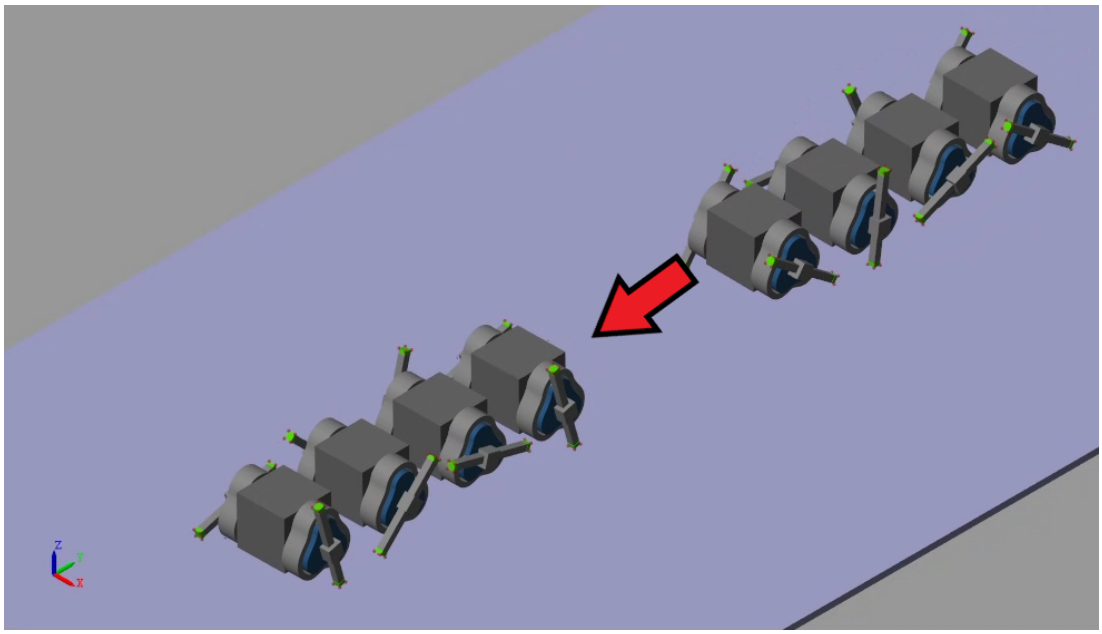

Figure 4.7: Snapshot of Simscape simulation. Green tips are force contact points. This simulation is of four body segment millipede-like gait

4.3.1 Conclusion on Simulation

The stability considerations of the robot were considered in several iterations, slowly growing more complex, beginning with an application of the kinematic equations derived in Chapter 2, and finalizing with a simulation environment developed in Simscape Multibody. The analysis between the kinematics and the Matlab simulation corroborate the conclusion that centipede locomotion with neighboring legs 60 degrees out of phase provide the most stable system. Though this section's data analysis of the Walker robot is limited to stability, the simulation environment developed in Simscape Multibody is a primary development of this paper. It is capable of providing more data points, with proven validity in the following chapter. The environment can measure data points, including the torque on each leg actuation joint, the speed of the robot, and provide a test harness for different body shapes.

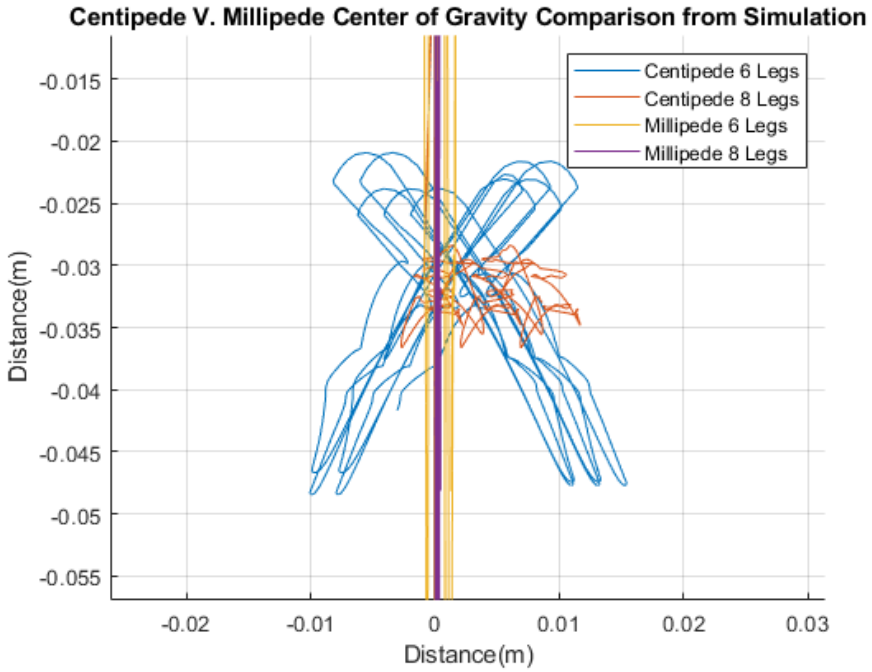

Figure 4.8: Center of gravity measurements from 10 second simulation, Millipede has greater horizontal stability, centipede has greater overall stability.

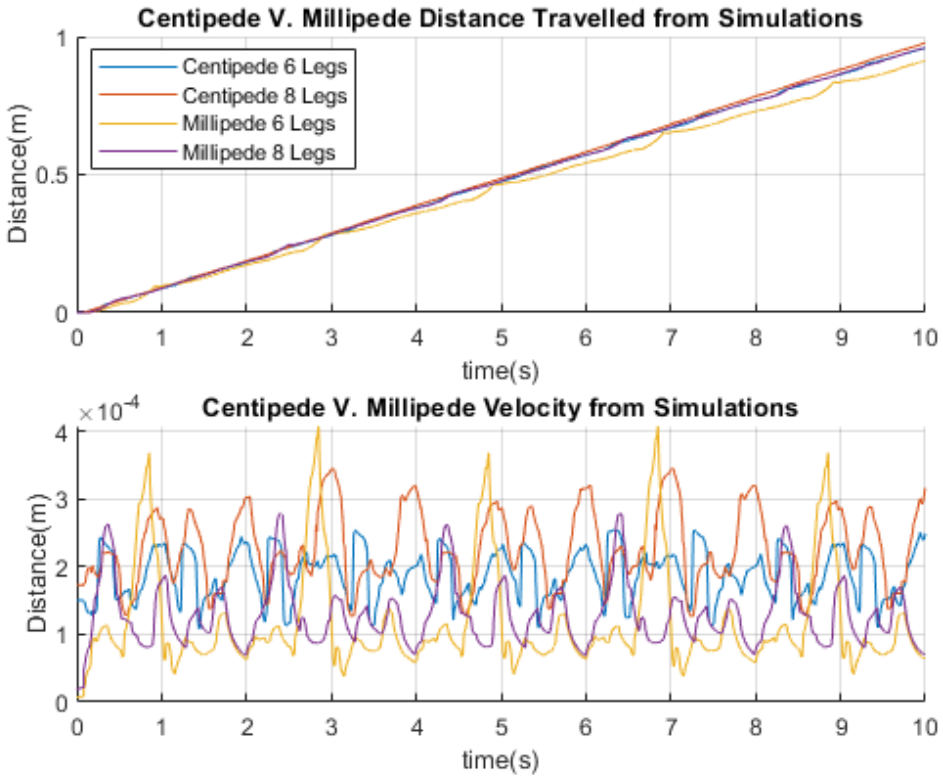

Figure 4.9: Distance travelled and velocity of simulations. Millipedes broadly moved slower than the centipede gait. Millipedes also had far greater variability in velocity

Chapter 5

Final Model and Conclusions

My research uses a Raised 3D Pro2 printer (see Fig. 5.1) using the software ideaMaker with a precision of 0.5 mm to print the Fusion 360 models of the cam leg design. Two design iterations were printed and attached to an Antrader Dual Shaft 3-6V Motor for testing. Section 5.1 discusses the manufacturing consideration of the actuation device and the following sections test the device, the goal of which is to prove the validity of the developed simulation environment in Section 4.2.

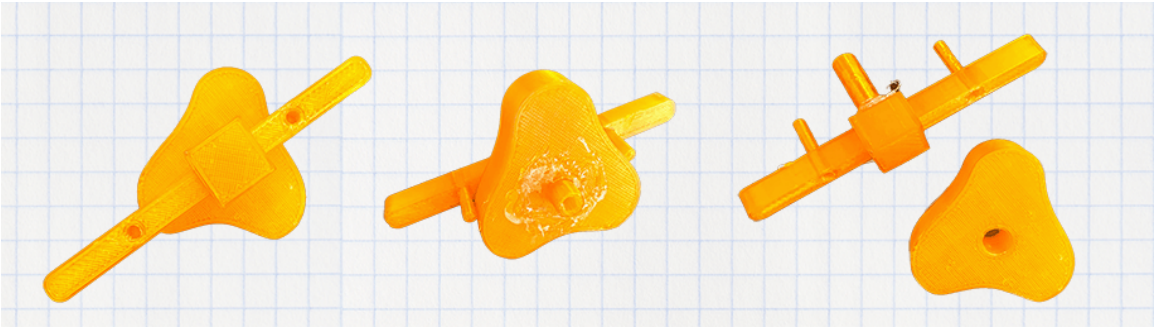

Figure 5.1: First cam print parts

5.1 Print Faults and Fixes

The specifications displayed in Fig. 3.21 define the first print of the design. The first iteration print of the design included the following faults:

- Unstable connection between the base of the rotating arm shaft and the leg insert, fixed in Fig. 5.3.

- Lack of mount. The cam had no built-in mechanism for mounting, fixed in Fig. 5.4
- Sharp contour edges, creating jerk when 3d printing. Fixed by rounding edges on the face of objects.

The second iteration of the print, the final print, proved to be sturdy after ameliorating the faults in the preceding list. To reduce print time, the interiors of the shapes contained several cardboard-like edges, in place of a complete infill, displayed in Fig. 5.2, which negligibly affected stability.

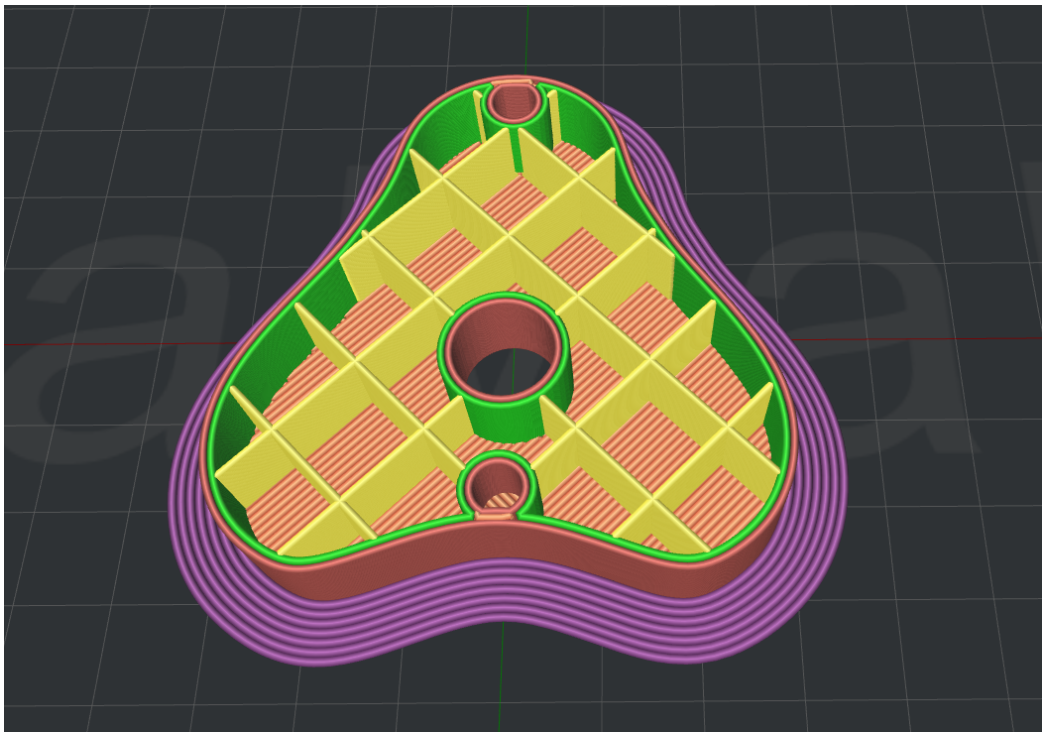

Figure 5.2: Interior slice of print. Reducing the amount of infill decreased print time while maintaining stability.

5.1.1 Conclusion on Print

Other manufacturing processes could avoid the issues that printing the mechanism created. Crow [3] manufactured a similar actuation device using metal which might be a more promising approach to build stability and the amount of material needed. Another manufacturing method might consider a multiple material design

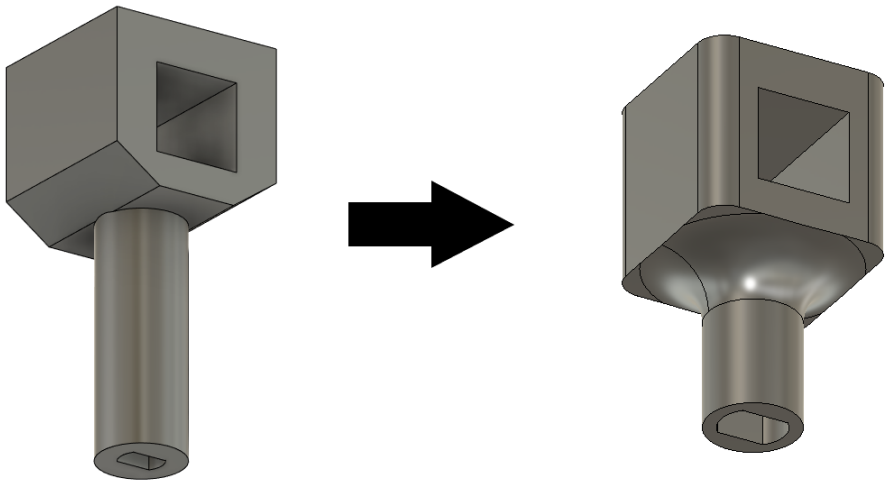

Figure 5.3: Change in rotary arm design: smoothed contour of shape, squared shape of leg slot, and added more connection material between base and shaft

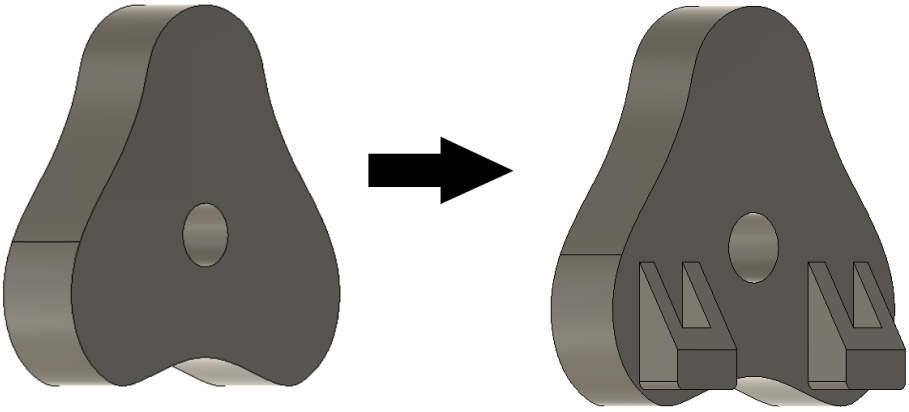

Figure 5.4: Change in cam design: decreased thickness of cam and added brackets for mounting

in which the cam is 3D plastic, and the rotary arm and legs are metal. The final print ameliorated most material issues, and the 3D plastic print proved to be exceptionally stable.

Widening the base of the rotary arm shaft created a more stable connection. Rounding the contours of the shape faces improved the consistency of print quality by reducing jagged edges, and the added mounts created a sturdy support surface. The only design change to consider is the frictional contact between the ends of the leg and the ground. In some cursory testing, frictional contact improved with glued rubber pieces to the ends of the leg. Another iteration of the design would expand

on better frictional contact.

5.2 Testing of Printed Leg

The objective of testing the leg mechanism with a limited budget is to acquire experimental data compared to the simulation data. Comparable data experimentally proves the developed Simscape Multibody simulation environment concerning the type of data obtained, i.e., gait dynamics. The primary test regime of the simulation environment is limited to the dynamic gait model of an omnipede-like robot using the designed cam leg mechanism.

The trajectory of the print is analyzed in Section 5.2.2 with discussion of failed testing systems in Section 5.2.4 and a short discussion of angular velocity in Section 5.2.5.

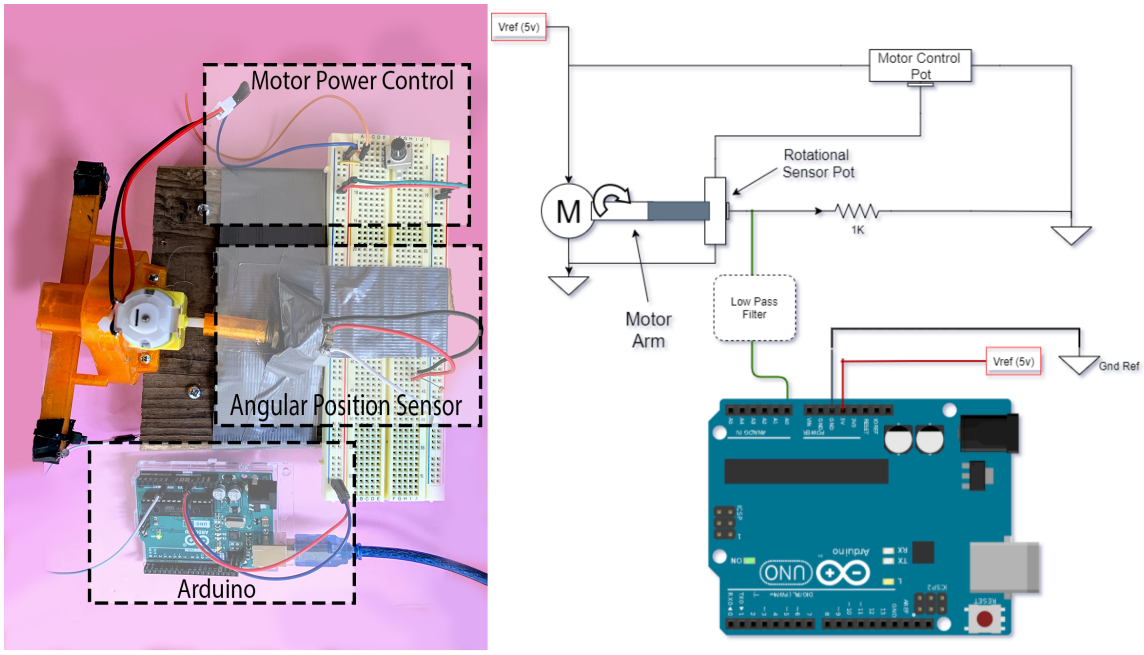

Figure 5.5: Test environment of device. On the right is the circuit diagram representation of the picture on the left. An Arduino was used for the test harness.

5.2.1 Consideration of Ideal Test Environment vs. Home-Brew Testing

As mentioned in prior sections, this research was conducted at home without laboratory equipment. This test environment limited my ability to collect rotational acceleration/position and frictional contact. Ideally, the relative angular position would be sensed with a quadrature encoder attached to the back arm of the motor, see Kano et al. [9] for some idea of how this would look. Kano's test environment mounted a motor on a surface above a conveyor belt capable of measuring thrust potential. Without the lab equipment, the attempt to measure frictional contact did not prove fruitful. The bulk of considered experimental data is dependent on the comparative trajectory analysis of the device using After Effects and the simulation data from Simscape Multibody.

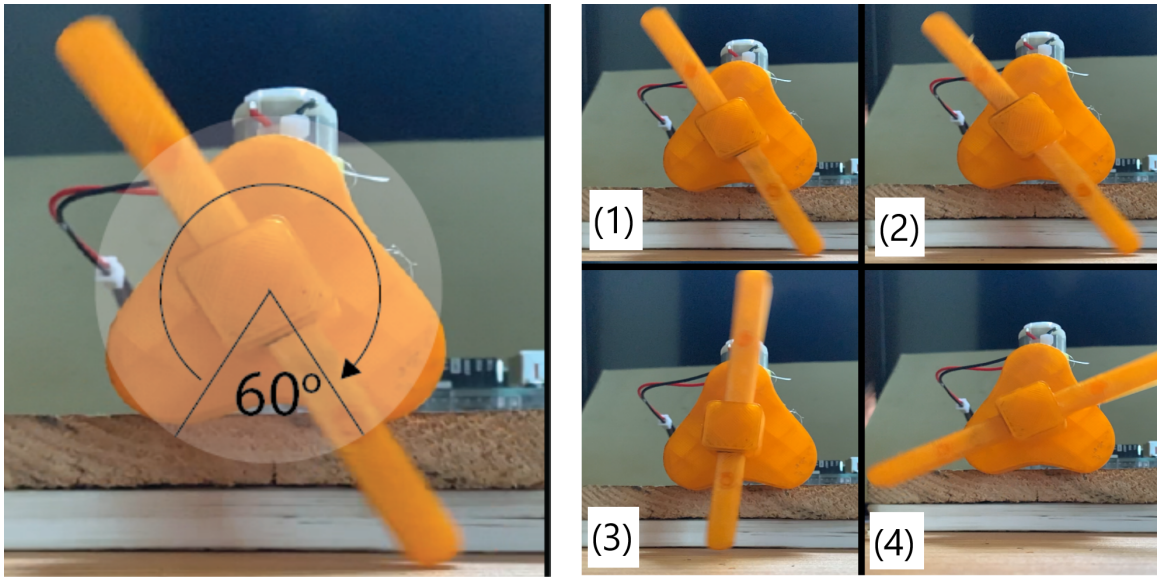

Figure 5.6: Sixty degree span of leg contact with ground. (1-4) show snapshot of the motion of the leg, which moved as initially intended.

5.2.2 Testing Trajectory

A test harness determines if the leg mechanism's trajectory is comparable to the intended orbit in the original design, shown in Fig. 3.18. The test system, shown in Fig. 5.5, is comprised of an Arduino Uno, a 10-spin potentiometer for angular

position detection, and a potentiometer in a voltage divider circuit to control the speed of the DC motor. The angular position of the leg was initially determined by reading the resistance of the 10-spin potentiometer connected to the shaft of the DC motor. This data was not used in the final trajectory analysis, though, as it proved to be quite noisy, as discussed in Section 5.2.4.1.

The trajectory was measured using After Effects motion tracking of a slow-motion video of the leg mechanism, see Fig. 5.8. This motion data does not include any time data, as an iPhone 8s with custom slow-mo software captured the slow-motion video. This issue hinders capturing angular velocity, discussed further in Section 5.2.3.

5.2.3 After Effects Trajectory Analysis

Fig. 5.6 shows the motion of the 3D printed leg in motion and the span of it's propulsive state. In the first trial, the system appeared to move as intended. After Effects motion-tracked a green dot on a piece of paper attached to the foot of the cam for one rotation. Analysis ignored velocity of the leg as tracking data returns the foot's position based on the frame data from the video, which is not a source for time data because of the custom iPhone slow-motion video capture software.

Typically, cameras record at a standard rate of 30 frames per second(fps), or possibly 60 fps, but the iPhone uses software that automatically slowed down parts of the video and added inconsistencies in using the frames as a determination of time. Fig. 5.7 shows the position of the trajectory without any reference to time. Angle of the arm is determined with trigonometry i.e. $\theta = \arcsin \frac{y_{pos}}{x_{pos}}$.

The ideal analysis would capture data in millimeters. My home laboratory setup, which uses After Effects only, provides pixel data; thus, I normalize the trajectory in pixels to the known length of the leg 120mm.

As shown in Fig. 5.8 the trajectory proves to be relatively accurate. Fig. 5.9 shows an error analysis.

The maximum error is about 4.6mm between 70 to 120 degrees. This error does not significantly impact the gait of the system, as it occurs at the bottom of the foot trajectory and maintains a visually straight course as shown in Fig. 5.7. Minor improvements would include a better mounting surface as well as larger pegs on the leg. The pegs used in the test were shorter than the width of the cam and had some tendency towards skewing.

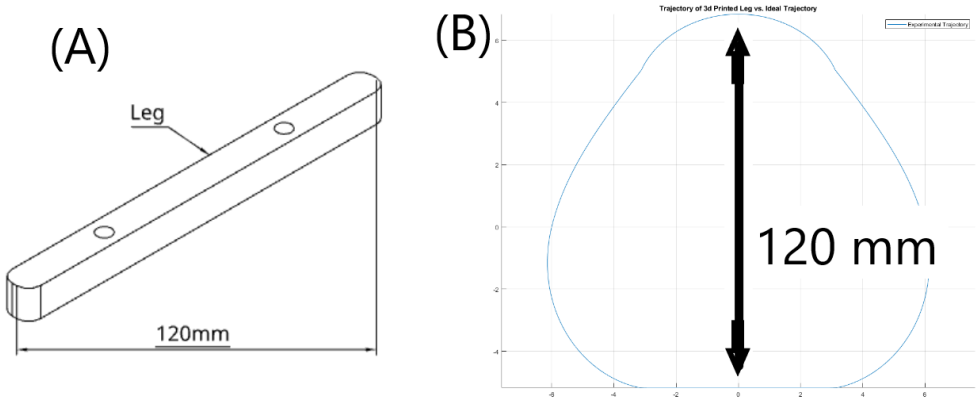

Figure 5.7: Normalized After Effects tracking motion compared to ideal motion. Length of the leg shown in (A) is known variable to normalize the tracking data shown in (B).

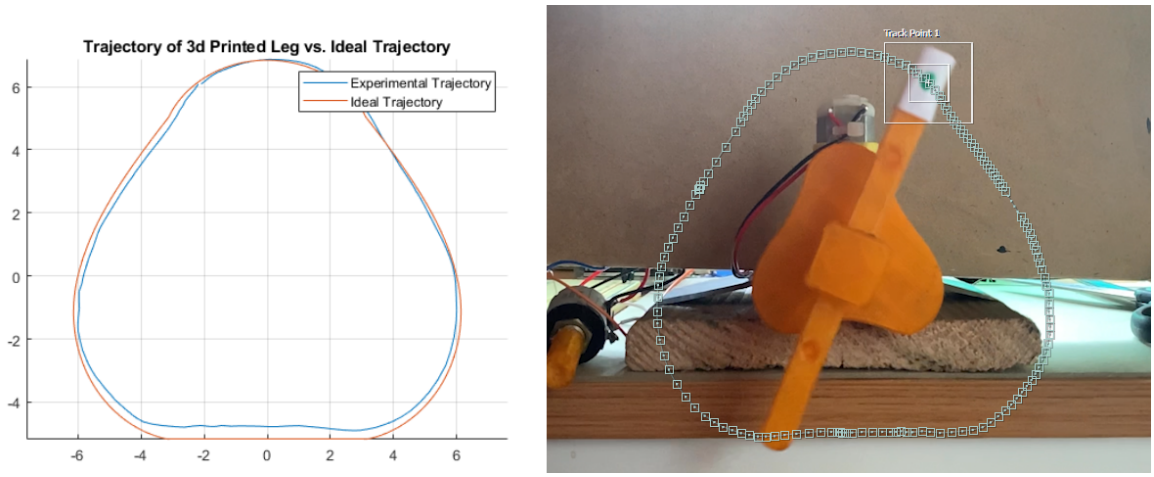

Figure 5.8: Normalized After Effects tracking Motion compared to ideal motion. Max error is $\approx$ 4.5mm.

5.2.4 Unsuccessful Test Environments

5.2.4.1 Potentiometer for Angular Position

There was an attempt to grab the angular position of the motor with a 10-spin potentiometer. The potentiometer proved to be significantly noisy enough to render the data unusable, see Fig. 5.10.

An attempt was made to reduce high frequency noise error with an RC low pass filter, as well as a running average, shown in Fig. 5.11, 5.12.

Both hardware and software low pass filters could not reduce noise enough to create a stable signal. Notwithstanding the overall instability of the signal, the low

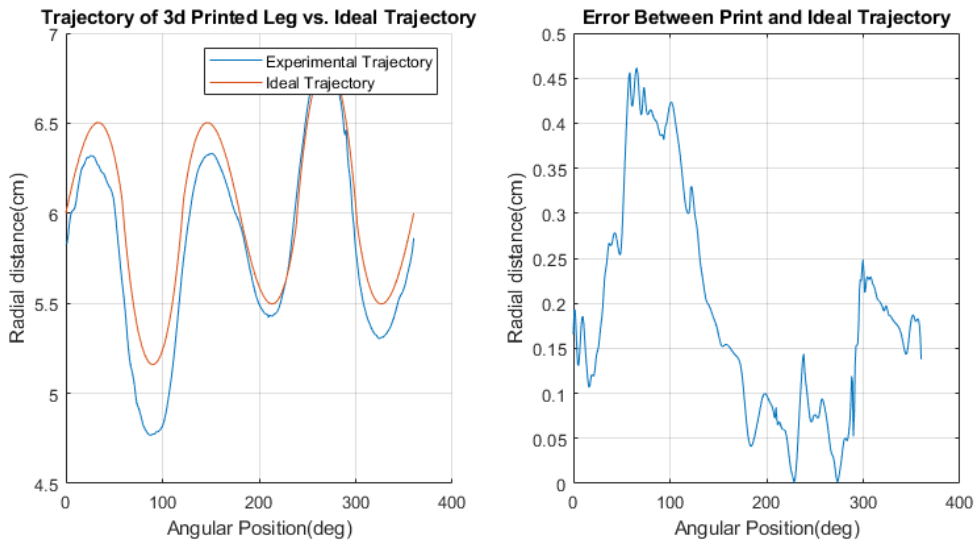

Figure 5.9: Normalized motion comparison to ideal. The right graph shows the difference between the two curves in the left graph.

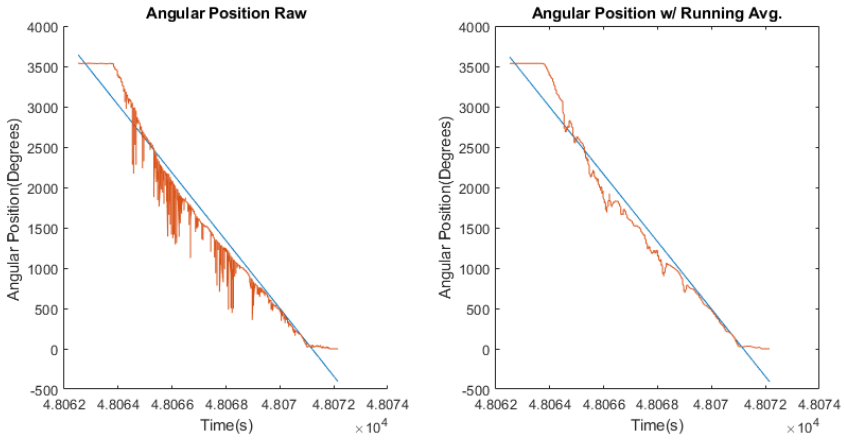

Figure 5.10: Data from potentiometer rotation sensor without any data filtering. Signal is very noisy, a running average is used to fix this.

pass filter with a 15Hz cutoff has near linearity at turns below approximately 500 degrees. This section of data roughly estimates the angular velocity of the leg. With a line of best fit of the data, we get that the approximate *angular velocity is -395.325 deg/second.*

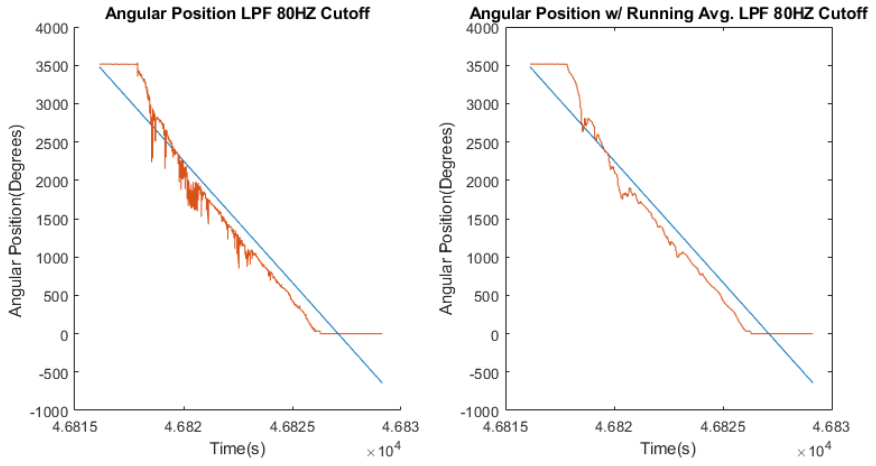

Figure 5.11: Data from potentiometer rotation sensor with an 80Hz cutoff low pass filter. Data is less noisy than the raw data but still not ideal.s

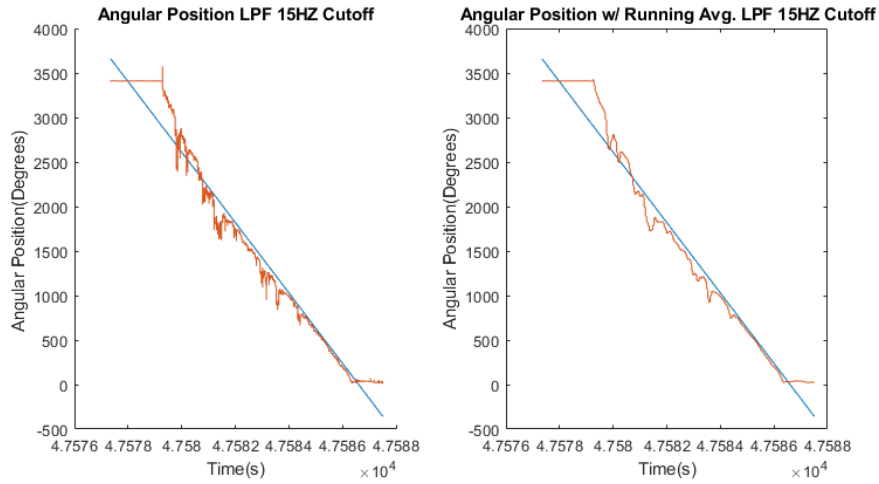

Figure 5.12: Data from potentiometer rotation sensor with 15 Hz cutoff low pass filter. Data is far less noisy but still isn't linear.

5.2.4.2 Inertial Measurement Unit for Linear Position

To analyze the frictional contact of the device, i.e., its ground contact, an Inertial Measurement Unit (IMU) was attached to a piece of long construction paper held below the mounted, rotating leg. When in contact, the leg pushed the paper much like a conveyor belt. This test harness also proved to be inadequate. Using the accelerometer on the MPU9250 IMU, with the highest polling rate, integrated accelerometer data found the paper's position on a single axis, i.e., $X_{pos} = \int \int \ddot{x}$.

However, integration of inaccurate data creates huge errors, so this method also failed, as shown in Fig. 5.13. The sensor was held on a level surface in the test and

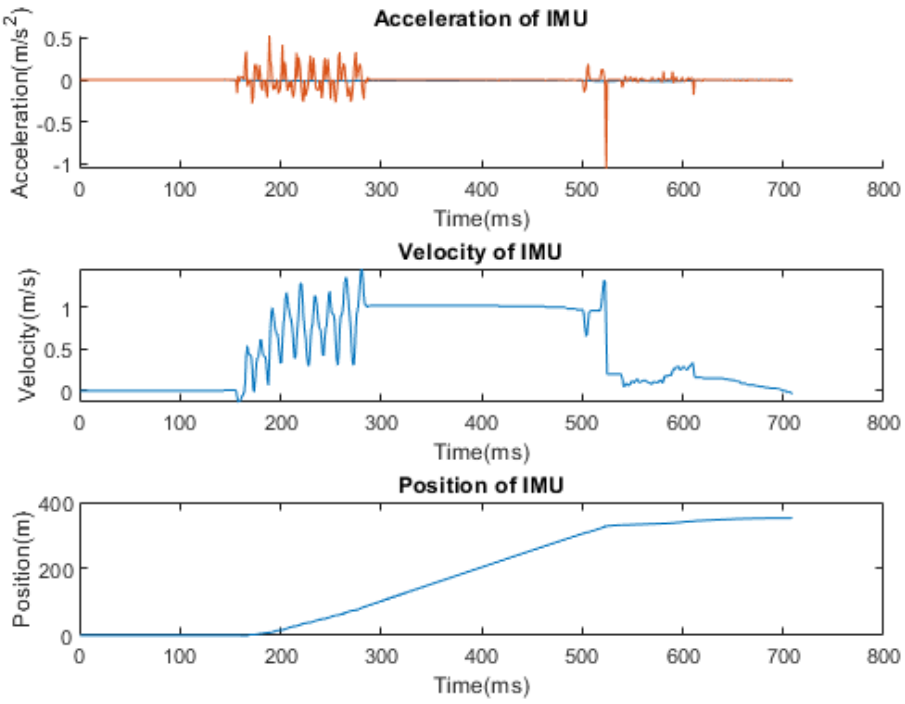

Figure 5.13: Data from MPU9250 IMU

slowly dragged forward and backward while measuring the acceleration. Accurate acceleration data should return the single-axis position to zero when reaching the origin, but the inaccuracy of the prevents this. Fig. 5.13 shows the velocity and position drift from the integration of inaccurate data.

5.2.5 Conclusion on Testing

The data gathered in this chapter provides confidence in the Simscape simulation environment. The foot trajectory of the device has a maximum error of 4.6 mm, falling short at the flat, propulsive portion of its path. As a product of Home-Brew development, this leg actuation device has proven to function within a negligible margin of its intended design. Measurement of the legs, such as angular velocity, acceleration, and torque, are not reliable data points generated by the simulation in

its current state. As supported by the completed tests simulation environment, the simulation represents an idealized dynamic gait model for the Walker robot. In future work, the model might stand as a more accurate model for the aforementioned data points through experimental proof and further development of the Simscape environment.

Fig. 5.14 shows a cursory observation of the angular position of the leg according to time. As mentioned in section 5.2.3 the frame rate of the camera might be variable, so this data should not be considered with complete confidence. Notwithstanding this source of error, we see in Fig. 5.14 that the simulation data is linear while the actual device drifts from linearity. Testing captured these data sets while the mechanism was suspended in the air, restricting any ground contact.

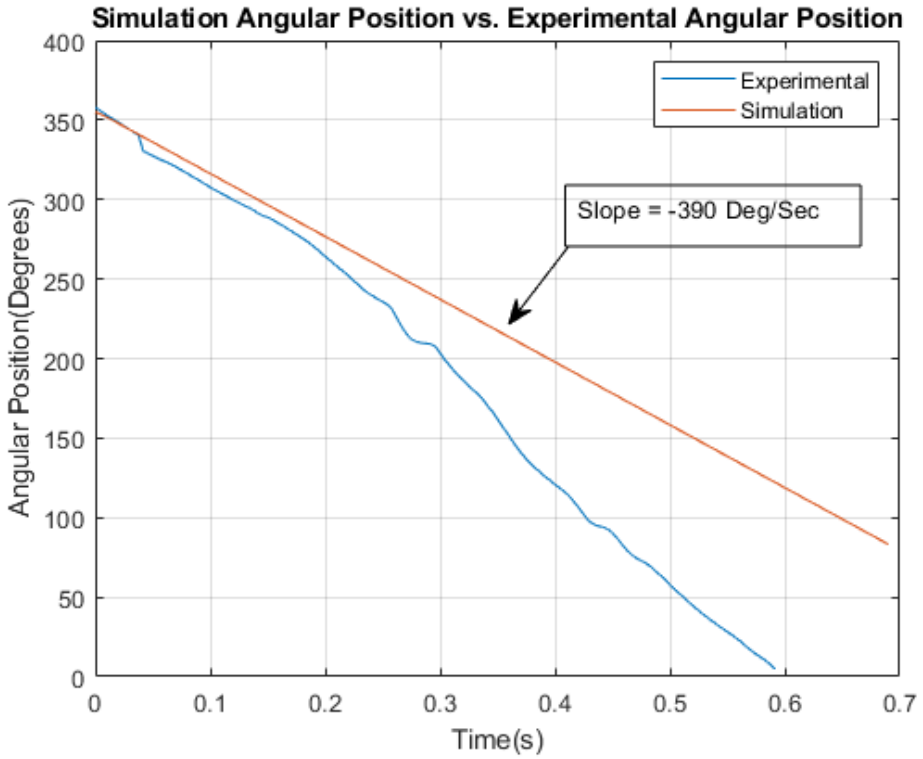

Figure 5.14: Comparison of simulation data to experimental data. The simulation data shows a constant slop that the experimental should maintain.

5.3 Conclusion

At the beginning of this paper, the goal was to explore the locomotion of millipede and centipedes as inspiration for a stable, affordable robot platform, implementing home-brew techniques for development, simulation, and analysis. In the observation of millipede vs. centipede locomotion through a literature review, studies like Manton [12][13], as well as Garcia et al. [5][7], and Kano et al. [9] investigated the thrust potential of the former and the speed of the latter. After considering several leg actuators, a novel, simple actuation device by Wan and Song [19] emulating the idealized gait kinematics of the Myriapoda developed by Sathirapongsasuti et al. [18] proved a robust leg mechanism for Walker.

This paper contributes to robotics and mechanical engineering, a literature review of omnipede gait kinematics and dynamics, and a simulation environment for omnipedes based upon Sathirapongsasuti's[18] kinematic model verified by austere sensor technology. Additional contributions include a robust and affordable prototype of the novel Wan and Song [19] leg actuator using modern manufacturing tools, previously manufactured by Crow [3] with limited success. Crow's design lacked the double-sided leg of the source paper, as well as any simulation. In the future, this actuator could replace bulky multi-motored locomotive systems not limited to just millipede motion.

5.3.1 Future Work

Future development of the Simscape simulation environment would include further study of chaotic terrain traversal through atypical terrain types and more emphasis on force analysis. Adding friction parameters that are experimentally verified to the leg components increases the region of reliable data the simulation can produce.

Expanding upon the already printed and proven effective leg actuation device, a full-bodied Walker would be a highly modular, inexpensive locomotion platform.

Bibliography

[1] B Anderson, J Shultz, and B Jayne. Axial kinematics and muscle activity during terrestrial locomotion of the centipede scolopendra heros. *Journal of experimental biology*, 198(5):1185–1195, 1995.

[2] S.D. Conte and C. De Boor. *Elementary Numerical Analysis: An Algorithmic Approach*. Classics in Applied Mathematics. Society for Industrial and Applied Mathematics, 2017. ISBN 9781611975192. URL https://books.google.com/books?id=tNBTDwAAQBAJ.

[3] Andrew Crow. cam controlled walking robot. 2005.

[4] Carl De Boor. *A practical guide to splines*, volume 27.

[5] Anthony Garcia, Shashank Priya, and Paul Marek. Understanding the locomotion and dynamic controls for millipedes: Part 1-kinematic analysis of millipede movements. In *Integrated System Design and Implementation; Structural Health Monitoring; Bioinspired Smart Materials and Systems; Energy Harvesting*, ASME 2015 Conference on Smart Materials, Adaptive Structures and Intelligent Systems, SMASIS 2015. American Society of Mechanical Engineers, 2015. doi: 10.1115/SMASIS2015-8894. ASME 2015 Conference on Smart Materials, Adaptive Structures and Intelligent Systems, SMASIS 2015 ; Conference date: 21-09-2015 Through 23-09-2015.

[6] Anthony Garcia, Gregory Krummel, and Shashank Priya. Fundamental understanding of millipede morphology and locomotion dynamics. *Bioinspiration & Biomimetics*, 16(2):026003, 2020.

[7] Anthony Jon Chanco Garcia. *Millipede-Inspired Locomotion for Rumen Monitoring through Remotely Operated Vehicle*. PhD thesis, Virginia Tech, 2018.

[8] Stephen P Hopkin, Helen J Read, et al. *The biology of millipedes.* 1992.

[9] Takeshi Kano, Kazuhiko Sakai, Kotaro Yasui, Dai Owaki, and Akio Ishiguro. Decentralized control mechanism underlying interlimb coordination of millipedes. *Bioinspiration & Biomimetics*, 12(3):036007, apr 2017. doi: 10.1088/1748-3190/aa64a5. URL https://doi.org/10.1088/1748-3190/aa64a5.

[10] Dooyeol Koh, Jaemin Yang, and Soohyun Kim. Centipede robot for uneven terrain exploration: Design and experiment of the flexible biomimetic robot mechanism. In *2010 3rd IEEE RAS & EMBS International Conference on Biomedical Robotics and Biomechatronics*, pages 877–881. IEEE, 2010.

[11] Geoffrey Long, Jay Anderson, and Johann Borenstein. The kinematic design of the omnipede: a new approach to obstacle traversion. In *Proceedings 2002 IEEE International Conference on Robotics and Automation (Cat. No. 02CH37292)*, volume 1, pages 714–719. IEEE, 2002.

[12] S. M. Manton. The evolution of arthropodan locomotory mechanisms.—part 4. the structure, habits and evolution of the diplopoda. *Journal of the Linnean Society of London, Zoology*, 42(286):299–368, 1954. doi: https://doi.org/10.1111/j.1096-3642.1954.tb02211.x. URL https://onlinelibrary.wiley.com/doi/abs/10.1111/j.1096-3642.1954.tb02211.x.

[13] Sidnie Milana Manton. The evolution of arthropodan locomotory mechanisms: Part 10. locomotory habits, morphology and evolution of the hexapod classes. *Zoological Journal of the Linnean Society*, 51(3-4):203–400, 1972.

[14] Alessandro Minelli. *The Myriapoda*. Brill, 2011.

[15] Alessandro Minelli. *Treatise on Zoology - Anatomy, Taxonomy, Biology. The Myriapoda, Volume 2*. Brill, Leiden, The Netherlands, 29 Sep. 2015. ISBN 978-90-04-18827-3. doi: https://doi.org/10.1163/9789004188273. URL https://brill.com/view/title/13488.

[16] Gary Parker and Jonathan Mills. Metachronal wave gait generation for hexapod robots. 02 1998.

[17] Marc H Raibert. *Legged robots that balance*. MIT press, 1986.

[18] Jarupon Sathirapongsasuti, Natdanai Punnanithi, and Poomyos Wimonkittiwat. Walking with a millipede. *Intel ISF*, 2004.

[19] Xiaonan Wan and Shin-Min Song. A cam-controlled, single actuator-driven leg mechanism for legged vehicles. volume Dynamic Systems and Control, Parts A and B of *ASME International Mechanical Engineering Congress and Exposition*, pages 1287–1292, 11 2004. doi: 10.1115/IMECE2004-62266. URL https://doi.org/10.1115/IMECE2004-62266.

[20] Heather M Wilson. Muscular anatomy of the millipede phyllogonostreptus nigrolabiatus (diplopoda: Spirostreptida) and its bearing on the millipede "thorax". *Journal of Morphology*, 251(3):256–275, 2002.

Please use the following page format for the cover of your report.

Walker: A Simple Millipede Bot

Thesis for the degree of

Bachelor of Science in Robotics Engineering

by

Kyle Jeffrey
1675663

DEPARTMENT OF ELECTRICAL AND COMPUTER ENGINEERING

UNIVERSITY OF CALIFORNIA SANTA CRUZ

SPRING 2021